Keratin 8 is a scaffolding and regulatory protein of ERAD complexes

Iwona M. Pranke[1*], Benoit Chevalier[1,#], Aiswarya Premchandar[3,#], Nesrine Baatallah[1], Kamil F. Tomaszewski[1], Sara Bitam[1], Danielle Tondelier[1], Anita Golec[1], Jan Stolk[4], Gergely L. Lukacs[5,6], Pieter S. Hiemstra[4], Michal Dadlez[3], David A. Lomas[7], James A. Irving[7], Agnes Delaunay-Moisan[8], Eelco van Anken[9], Alexandre Hinzpeter[1, #], Isabelle Sermet-Gaudelus[1,2, #], Aleksander Edelman[1*]

1 Inserm, U1151 - CNRS UMR 8253 – Université de Paris, Paris, France

2 Cystic Fibrosis Center, Hôpital Necker Enfants Malades, Assistance Publique Hôpitaux de Paris, France

3 Laboratory of Mass Spectrometry, Institute of Biochemistry and Biophysics, Polish Academy of Sciences, PL-02106, Warsaw, Poland

4 Department of Pulmonology, Leiden University Medical Center, Leiden, the Netherlands

5 Department of Physiology, McGill University, Montréal, Quebec, Canada

6 Department of Biochemistry, McGill University, Montréal, Quebec, Canada

7 UCL Respiratory and the Institute of Structural and Molecular Biology, University College London, London WC1E 6JF, United Kingdom

8 Université Paris-Saclay, CEA, CNRS, Institute for Integrative Biology of the Cell (I2BC), Gif-sur-Yvette, France

9 Division of Genetics and Cell Biology, San Raffaele Scientific Institute, Milan, Italy

*** Corresponding authors**: Edelman Aleksander; Inserm U1151 - CNRS UMR 8253 – Université de Paris– 156 – 160 rue de Vaugirard - 75015 Paris, France; aleksander.edelman@inserm.fr; Tel: (033) 01 72 60 64 10

Pranke Iwona Maria; Inserm U1151 - CNRS UMR 8253 – Université de Paris– 156 – 160 rue de Vaugirard - 75015 Paris, France; iwona.pranke@inserm.fr; Tel : (033) 01 40 61 53 32

Equally participated

Key words:

Intermediary filaments, cytoskeleton, protein-protein interaction, protein complexes fractionation, synthetic lethality, epithelium

Abstract

Early recognition and enhanced degradation of misfolded proteins by the endoplasmic reticulum (ER) quality control and ER-associated degradation (ERAD) cause defective protein secretion and membrane targeting, as exemplified for Z-alpha 1 antitrypsin (Z-A1AT), responsible for alpha-1-antitrypsin deficiency (A1ATD) and F508del-CFTR (cystic fibrosis transmembrane conductance regulator) responsible for cystic fibrosis (CF).

Prompted by our previous observation that decreasing Keratin 8 (K8) expression increased trafficking of F508del-CFTR to the plasma membrane, we investigated whether K8 impacts trafficking of soluble misfolded Z-A1AT protein. The subsequent goal of this study was to elucidate the mechanism underlying the K8-dependent regulation of protein trafficking, focusing on the ERAD pathway.

The results show that diminishing K8 concentration in HeLa cells enhances secretion of both Z-A1AT and wild type (WT) A1AT with a 13-fold and 4-fold increase, respectively. K8 down-regulation triggers ER failure and cellular apoptosis when ER stress is jointly elicited by conditional expression of the μ_s heavy chains, as previously shown for Hrd1 knock-out. Simultaneous K8 silencing and Hrd1 knock-out did not show any synergistic effect, consistent with K8 acting in the Hrd1-governed ERAD step. Fractionation and co-immunoprecipitation experiments reveal that K8 is recruited to ERAD complexes containing Derlin2, Sel1 and Hrd1 proteins upon expression of Z/WT-A1AT and F508del-CFTR. Treatment of the cells with c407, a small molecule inhibiting K8 interaction, decreases K8 and Derlin2 recruitment to high-order ERAD complexes. This was associated with increased Z-A1AT secretion in both HeLa and Z-homozygous A1ATD patients' respiratory cells. Overall, we provide evidence that K8 acts as an ERAD modulator. It may play a scaffolding protein role for early-stage ERAD complexes, regulating Hrd1-governed retrotranslocation initiation/ubiquitination

processes. Targeting K8-containing ERAD complexes is an attractive strategy for the pharmacotherapy of A1ATD.

Introduction

Proper protein folding represents one of the primary challenges for cells to maintain proteostasis. This complex process is challenged by the intrinsic properties of proteins or mutations in protein-coding genes. Proteins entering the secretion pathway that fail to fold, assemble or post-translationally mature properly are eliminated by ERAD. ERAD relies on multiple dynamic protein complexes acting sequentially to recognise, tether, ubiquitin-tag and extract misfolded substrates from the ER, thereby enabling their proteasomal degradation in the cytosol (Christianson and Ye, 2014) (Mehrtash and Hochstrasser, 2019) (Ruggiano et al., 2014). Distinct ERAD pathways accommodate the variety of topologies and post-translational modifications encountered in misfolded protein substrates. The partial redundancy of ERAD factors allows cells to oversee proteostatic stress and maintain ER homeostasis coordinately. ERAD pathways can be divided into the following functional modules: (i) substrate recognition; (ii) retro-translocation initiation with substrate unfolding involving mainly multifunctional Derlin proteins; (iii) ubiquitination of the partially dislocated substrate, assisted by different membrane-bound E3 ubiquitin ligases (e.g. a multimeric complex, containing Hrd1 E3 ligase coupled to substrate recognition protein Sel1) and associated ubiquitin-conjugating enzymes E2s according to substrates (Baldridge and Rapoport, 2016) (Stein et al., 2014) (Vasic et al., 2020); therefore licensing (iv) the dislocation process ensured by p97/VCP ATP-ase providing a pulling force (Garza et al., 2009) (Nakatsukasa et al., 2008) (Rabinovich et al., 2002); and finally (v) substrate degradation by 26S proteasome.

Protein misfolding underlies two frequent pulmonary genetic diseases, A1ATD and CF. The most common disease-causing protein folding mutations are Glu342Lys (Z) in A1AT and F508del in CFTR (Kerem et al., 1989) (Stoller and Aboussouan, 2012) (Ghouse et al.,

2014). Over 99% of F508del-CFTR and ~70% Z-A1AT are degraded by ERAD (Jensen et al., 1995) (Teckman et al., 2001) (Kroeger et al., 2009a). Both misfolded proteins form complexes with ER-chaperones (e.g., Calnexin) (Kim and Skach, 2012) (Schmidt and Perlmutter, 2005), ubiquitin ligases (e.g., Hrd1 and its partner Sel1) (Lomas et al., 1992) (Khodayari et al., 2017a) (Glenn et al., 2012) (Shen et al., 2006) (Graham et al., 1990), and dislocating protein p97/VCP (Perlmutter, 2006) (Khodayari et al., 2017b) (Carlson et al., 2006). Consequently, misfolded F508del-CFTR is less efficiently targeted to the apical membrane (PM) of epithelial cells and secretion of misfolded Z-A1AT is strongly decreased (to ~10–15% of WT level). In addition, the folding efficacy of WT-CFTR is limited as observed in heterologous overexpressing system, but not clearly confirmed in native tissue (Okiyoneda and Lukacs, 2012) (Okiyoneda et al., 2013), and the thermodynamic state of WT-A1AT is suboptimal (Chakraborty and Teckman, 2014), both features favouring ERAD degradation of the WT isotypes (Varga et al., 2004). Additionally, for Z-A1AT, which is highly expressed in the hepatocyte, its accumulation in the ER also activates classic autophagy (Kroeger et al., 2009a) and ER-to-lysosome-associated degradation (Fregno et al., 2018).

An increasing body of evidence suggests that K8 and Keratin 18 (K18), proteins forming intermediary filament (IF) heterodimers in simple epithelia (Herrmann and Aebi, 2004), can regulate protein targeting to the apical plasma membrane (Coulombe and Omary, 2002) (Toivola et al., 2004) (Mashukova et al., 2016). They also display additional roles beyond mechanical and structural functions, including protein polyubiquitination in a pro-inflammatory context (Dong et al., 2016) or Akt-signaling regulation (Lim et al., 2021). Our previous studies (Davezac et al., 2004) (Colas et al., 2012a) revealed that K8 and K18 regulate F508del-CFTR trafficking. We have determined that K8 favoured F508del-CFTR retention in the ER (Colas et al., 2012b), an effect that can be alleviated pharmacologically

with small molecules, e.g., c407 (Odolczyk et al., 2013), and/or reducing K8 concentrations by siRNA (Colas et al., 2012a).

Here we show that K8 regulates the secretion of Z-A1AT. Since K8 affects the targeting of two ERAD substrates, Z-A1AT and F508del-CFTR, we challenged the hypothesis that K8 is part of the ERAD pathway. We gathered genetic and biochemical clues pointing to a new physiological function of K8 during the ERAD process. As for significant ERAD components (Hrd1, Sel1) (Vitale et al., 2019) in conditions triggering ER stress, we observed that K8 is essential to prevent ER failure and associated cell death. K8 co-sedimented and co-precipitated with major ERAD components (Derlin2, Hrd1 and Sel1), consistent with K8 acting as a scaffold in the Hrd1-dependent ERAD pathway. Finally, we provide proof of concept that modulation of K8-containing ERAD complexes increases Z-A1AT secretion from HeLa, and patients derived primary human respiratory epithelial (HNE) cells and could be a target for pharmacotherapy in A1ATD.

Results

1. Silencing K8 expression increases WT-A1AT and Z-A1AT secretion through the conventional secretory pathway

The implication of K8 in the secretion of WT-A1AT and misfolded Z-A1AT was evaluated in HeLa cells upon reduced K8 levels (shRNAK8, see Material and Methods section) (**Fig. 1A and B)**. Quantification of A1AT in the supernatants of control and shK8 cells showed significantly enhanced secretion of both Z-A1AT and WT-A1AT in shK8 cells (**Fig . 1B, lane numbers 1 and 2 for both A1AT WT and Z**), with a 13-fold and 4-fold increase of secretion, respectively (**Fig. 1B lane numbers 1 and 2 for both A1AT WT and**

Z). This secretion was associated with an increased intracellular pool of Z-A1AT (**Fig. 1C and D, lane numbers 1 and 2**), suggesting its stabilisation.

The enhanced WT- and Z-A1AT secreted by shK8 cells had an identical SDS-gel migration pattern compared to WT- and Z-A1AT secreted by control cells (**Fig. 1A, lane number 1 *vs.* 2 for both A1AT WT and Z,** shRNAK8- *vs.* shRNAK8+), indicative of a similar glycosylation pattern and secretion occurring through the conventional secretory pathway. This was confirmed using Brefeldin A (BFA), an inhibitor of the conventional secretory pathway, which abolished WT-/Z-A1AT secretion from both control and shK8 cells (**Fig. 1A and B**). Upon BFA treatment, an increase of Z- and WT-A1AT intracellular concentrations was observed in shK8 cells compared to control cells (**Fig. 1C and D**), consistent with reduced degradation of WT-/Z-A1AT upon decreased K8 expression.

To determine if the observed increase in WT- / Z-A1AT secretion was not linked to a general effect on proteins secretion, we performed several series of control experiments: (i) quantification of the secretome protein content did not differ in shK8 and K8-expressing (control) HeLa cells (**Supp. Fig. 2A**); (ii) secretion of transfected *Gaussia* luciferase was not modified (**Supp. Fig. 2B**); (iii) secretion of ER protein, BiP, both from control and shRNA K8 cells was not detectable by Western blot **(Supp. Fig. 2C**); (iv) expression of endogenous Na^+K^+ATPase at the plasma membrane was not changed upon K8 silencing (**Supp. Fig. 2D**); (v) secretion of heavy chain subunit μ_s of secretory IgM from control and shRNA K8 cells was not detectable (**Supp. Fig. 2E**); and (vi) there was no change in ER and secretory proteins in the secretome of shRNA K8 cells compared to control cells (**Supp, Fig. 2F**). Altogether these experiments suggest that K8-dependent regulation of secretion was specific of misfolded Z-A1AT or unstable WT-A1AT.

The accumulation of Z-A1AT upon BFA treatment in shK8 cells suggests an implication of K8 in the degradation *via* the ERAD or the autophagy pathways (Kroeger et al., 2009b). To test for a possible role of K8 silencing in rescuing Z-A1AT from autophagy, the effect of Wortmannin (1μM, 24h), an inhibitor of phosphoinositide 3-kinases, was tested. Intracellular accumulation of non-mature Z-A1AT upon treatment was observed without increased secretion (**Supp. Fig. 3A**). Autophagy induction by MK-2206 (5 μM, 20h), an inhibitor of Akt signaling pathway, did not increase A1AT secretion from both normal and shRNAK8 cells (**Supp. Fig. 3B**). Thus, the increase of A1AT secretion upon K8 silencing does not result from the autophagy pathway. On the other hand, a slightly increased expression of Grp78/BiP was observed (**Supp. Fig. 3C**) in shK8 cells, supporting a potential implication of K8 in the ERAD pathway. This is not due to the ER stress as another marker of ER stress, CHOP, was not changed (**Supp. Fig. 3C**) suggesting that BiP increase may be linked to K8 silencing which potentially influences the ER processes.

2. K8 is a critical factor for ERAD of μ_s

To evaluate the potential role of K8 in ERAD, we took advantage of a cellular model system expressing the heavy chain μ_s subunit of secretory IgM. There, the lethal accumulation of μ_s in the ER due to the absence of the light chain to enable antibody reconstitution and secretion is counterbalanced by enhanced ERAD degradation. The implication of K8 in the degradation of μ_s was monitored via cell death upon K8-silencing (synthetic lethality assay or growth assay, see Methods section for details).

K8 silencing triggered synthetic lethality of μ_s-expressing cells (**Fig. 2A**; siK8+μ_s). None of the other conditions (siRNA against K8 alone (siK8–μ_s)) and μ_s expression alone (ctrl+μ_s) led to significant cell death, asserting the features of *bona fide* synthetic lethality (**Fig. 2A**).

These results showed that decreasing K8 levels in μ_s-expressing cells led to their decreased viability, probably by compromising the ERAD pathway and overload of ER with μ_s.

3. K8 regulates Hrd1-dependent processes

We then searched for the ERAD process affected by K8 silencing. It has been previously shown that misfolded Z-A1AT secretion is not increased by inhibiting the proteasome (Teckman et al., 2001). We thus focused on ERAD steps governed by Hrd1 and p97/VCP (**Supp. Fig. 1,** Modules 2B and 3).

Knocking out Hrd1 in HeLa cells (stable Hrd1KO HeLa cells) (Vitale et al., 2019) increased Z-A1AT and WT-A1AT secretion (**Fig. 2B**), as already shown by Joly et al. (2017) for Z-A1AT. It was accompanied by increased levels of fully-glycosylated Z- and WT-A1AT in Hrd1KO cells (**Fig. 2B**). Therefore, disruption of the Hrd1 complex and consequently inhibition of substrate ubiquitination/retrotranslocation (**Supp. Fig. 1**, module 2A and 2B) appears to be an essential step favouring both WT-A1AT and Z-A1AT secretion.

To further investigate this question, we examined whether K8 is involved in the ERAD processes controlled by Hrd1. The effect of combining Hrd1KO and siRNAK8 was evaluated using synthetic lethality and A1AT secretion assays. Hrd1KO cells showed a significant synthetic lethality of cells upon μ_s induction (ctrl, siRNAK8, and scramble), underlining the importance of Hrd1 (**Fig. 2C**). When combining Hrd1KO and siRNAK8, no additive or synergistic effect was observed in synthetic lethality (**Fig. 2C**) or increased WT- /Z-A1AT secretion (**Fig. 2D**). The effect of K8 KD was stronger (**Fig. 2D**) suggesting potential regulation of multiple proteins of the ERAD complex. Both growth and secretion assays showed that Hrd1 and K8 modulate the secretion of WT- /Z-A1AT *via* the same pathway.

Pharmacological inhibition of VCP/p97 protein with Eeyarestatin I or NMS-873 was performed to test for the role of substrate dislocation (**Supp. Fig. 1**, module 3) on WT-/Z-A1AT secretion (**Supp. Fig. 4 A and B**). Both inhibitors led to the intracellular accumulation

of Z-A1AT and WT-A1AT, consistent with reduced degradation. Nonetheless, this was not associated with increased WT-/Z-A1AT secretion **(Supp. Fig 4** A and B, Secretion panels and quantification), indicating that the inhibition of substrate dislocation was insufficient to enhance secretion.

The observations above emphasised (i) the relationship between K8 and Hrd1 and (ii) the absence of increased secretion upon p97 inhibition, suggesting that K8 modulates early ERAD processes, i.e., Hrd1-dependent ubiquitination and initiation of retrotranslocation (**Supp. Fig. 1**).

4. K8 is recruited to ERAD complexes

For further insight into the involvement of K8 into ERAD processes, we determined if K8 is recruited to the ERAD complexes by performing sucrose gradient fractionations of ERAD complexes. The distribution of K8 and three important proteins of the Hrd1 complex (Hrd1, Sel1 and Derlin 2; **Supp. Fig. 1,** modules 2A and B) was monitored in mock-transfected cells and cells expressing WT-, Z-A1AT or μ_s.

In mock-transfected cells, K8 was primarily associated with lower sedimentation fractions (3-6) together with Derlin2 and a smaller amount of Sel1 **(Fig. 3A-C**). This suggested that K8 forms complexes, at the least, with Derlin2 and Sel1 (**Fig. 7**).

Expression of either Z-A1AT, μ_s, or WT-A1AT, shifted K8 (**Fig. 3A**) together with Derlin2, Sel1 and Hrd1 (**Fig. 3B-D**) toward heavier fractions compared to mock-transfected cells. This is consistent with the dynamic recruitment of K8 to different higher-order ERAD complexes upon expression of an ERAD substrate (**Fig. 7**). The observed differences in the distribution of WT-A1AT, Z-A1AT and μ_s proteins in sucrose gradients may be due to the differences in the recruitment of these proteins to degradation processes (**Fig. 3E**).

The existence of ERAD complexes including K8 was further validated by co-immunoprecipitation experiments performed in both polarized primary HNE cells

endogenously expressing Z-A1AT (**Fig. 3F**) and HeLa cells transfected with WT or Z-A1AT **(Supp. Fig. 4C)**. Derlin2, Hrd1 and Sel1 proteins were detected in immuno-precipitates of K8 and conversely K8, Hrd1 and Sel1 were co-immunoprecipitated with Derlin2.

To test if K8 influenced the formation of the ERAD complexes, we performed fractionation experiments on proteins obtained from shK8 mock- and shK8 Z-A1AT-transfected cells (**Fig. 4**). Under shK8 conditions, the total residual K8 co-sedimented with Derlin2 to one low-density fraction, unmasking a possible Derlin2-K8 complex (**Fig. 4A and B**, shK8 lines for K8 and Derlin2, black arrows). Profiles of Hrd1 and Sel1 fractionation were similar in mock-transfected and shK8 cells (**Fig. 4C and D**, compare lines shK8 and mock for Hrd1 and Sel1), suggesting that K8 does not influence the formation of complexes with Hrd1 and Sel1 under these conditions. The importance of K8 for the recruitment of Hrd1 and Sel1 to higher density complexes appeared on fractionation profiles of proteins derived from Z-A1AT expressing cells with normal and decreased levels of K8 (**Fig. 4C and D**). Noteworthy was that Hrd1 and Sel1 amounts were reduced in fraction 12 of the shK8 Z-A1AT sedimentation profile compared to cells expressing normal levels of K8 (**Fig. 4C and D**, red boxes). This shows that K8 favoured the recruitment of Hrd1 and Sel1 to high-order complexes under the expression of Z-A1AT.

Co-staining of K8 and Calnexin (CNX) showed a redistribution of K8 to the vicinity of the ER in Z-A1AT-expressing cells *vs.* WT-A1AT and mock-transfected cells (**Supp. Fig. 5A**). K8 co-distributed with Z-A1AT in HeLa and primary HBE cells as shown by immunocytochemistry (**Supp. Fig. 5B and C**) and proximity ligation assay (**Supp. Fig. 6A and B**). K18 also co-distributed with WT and Z-A1AT but without the increased proximity to Z-A1AT, in contrast to what was observed for K8 (**Supp. Fig. 6C**). Subcellular fractionation (**Supp. Fig. 6D**) showed that K8 association with ER-containing microsomes (attested by the presence of Calreticulin, **Supp. Fig**. **6E**) was enriched in Z-A1AT-expressing cells. Finally,

Proteinase K assay experiments (Besingi and Clark, 2015) excluded intra-ER localisation of K8 (**Supp. Fig. 6E**) as it was fully digested in both the presence and absence of detergent, a feature consistent with the reported cytosolic localisation of K8 (according to Human Protein Atlas and (Coulombe and Wong, 2004)). Altogether, these observations are consistent with sucrose gradient fractionation results described above and support the implication of K8 in the degradation processes within ERAD.

To test whether other misfolded proteins recruited K8 to ERAD complexes, we conducted sucrose gradient fractionations of samples from WT-CFTR and F508del-CFTR-expressing 16HBE14o-cells. Analysis of protein complexes (**Fig. 5**) showed that Derlin2, Hrd1 and K8 shifted towards heavier fractions (**Fig. 5A – D**) upon F508del-CFTR expression compared to WT-CFTR, similar to that observed for Z-A1AT and μ_s (**Fig. 3A, B and D**). Noticeably, the Sel1 shift to heavier fractions was weaker on F508del-CFTR than Z-A1AT, WT-A1AT and μ_s. The less pronounced shift of Sel1 towards high-density fractions upon F508del-CFTR expression could be explained because F508del-CFTR is expressed at an endogenous level compared to transiently transfected Z-A1AT. Recruitment of K8 to ERAD complexes was supported by co-immunoprecipitation of K8 with Derlin2 and Hrd1 from lysates of 16HBE cells expressing WT or F508del-CFTR (**Fig. 5 E**).

Altogether, the results obtained for misfolded Z-A1AT and F508del-CFTR demonstrated that the delivery mechanism to degradation depends on K8 recruitment to the ERAD complexes (**Fig. 7**).

5. A small molecule, c407, increases the secretion of Z-A1AT and is an ERAD modulator

To test if K8-containing ERAD complexes were druggable, we measured the WT-A1AT/Z-A1AT secretion upon treating HeLa and primary human nasal epithelial (HNE) cells

with the c407 compound, previously found to disrupt K8 - F508del-CFTR interaction and to correct CFTR trafficking to the plasma membrane (Odolczyk et al., 2013). Treatment of both cell types resulted in an increase of Z-A1AT secretion in the concentration range of 10-35 μM (**Fig. 6A and B**), 20 μM c407 being the most efficient. In both primary HNE and HeLa cells, c407 did not affect WT-A1AT secretion.

To test whether c407 targeted K8 directly, structure stabilisation experiments were performed using HDex-MS (hydrogen-deuterium exchange mass spectrometry) on purified K8. The addition of c407 (**Supp. Fig. 7A and B**) induced the stabilisation of multiple regions of K8, suggesting c407-K8 direct interactions. In solution, K8 was shown to exist as dimers in two distinct forms - a folded dimeric form stabilised by head-rod domain interactions and an unfolded dimeric form, as demonstrated by HDex-MS analysis (Premchandar et al., 2015). The robust allosteric stabilisation observed in the K8 head domain peptide 2-19 (**Supp. Fig 7A**, first panel) and the rod domain peptides (**Supp. Fig. 7A and B**) suggest a likely shift in the equilibrium to the folded form of the K8 dimer. These results were supported by observations from immunocytochemistry experiments showing partial recovery of K8 network after c407 treatment in HeLa cells expressing Z-A1AT and 16HBE cells expressing F508del-CFTR (**Supp. Fig. 8A and B**). Sucrose gradient fractionation of c407 treated HeLa cell lysates showed a less important shift of K8 and Derlin2 to heavy fractions compared to untreated cells (**Fig. 6C**), while Hrd1 and Sel1 were not affected. Moreover, Derlin2 co-distributed with K8 both in control conditions and after treatment with c407 according to immunocytochemistry (**Supp. Fig.8C and D**). Altogether, these results suggest that targeting the K8 - Derlin 2 complex with c407 enhances Z-A1AT secretion.

Discussion

In this study, we shed light on a new role of K8 as a scaffolding factor of ERAD protein complexes in epithelial cells (**Fig. 7**). We demonstrated that K8 negatively regulates secretory trafficking of misfolded Z-A1AT, as it was the case for F508del-CFTR (Colas et al., 2012a). Consequently, decreased K8 expression compromised ERAD leading to enhanced apoptosis of heavy chain μ_s-expressing cells. Finally, in three cell models, HeLa, HBE and polarized primary HNE cells, we provided evidence of K8 implication in the ERAD processes by demonstrating K8 recruitment to complexes containing Derlin2, Hrd1 and Sel1 proteins and thus modulation of Hrd1-orchestrated processes (**Fig. 7**). Altogether, these data suggest that K8 participates in retrotranslocation initiation and ubiquitination of Z-A1AT, F508del-CFTR, μ_s and to some extent WT-A1AT and WT-CFTR. This unveils new structural and regulatory features of K8 within ERAD.

Misfolded Z-A1AT and F508del-CFTR are in soluble complexes with multiple ER chaperones (Schmidt and Perlmutter, 2005) (Kim and Skach, 2012). They are substrates for the ERAD pathway (Baldridge and Rapoport, 2016) (Vasic et al., 2020) (El Khouri et al., 2013) orchestrated by Hrd1-dependent ubiquitination at an early step (Wang et al., 2011) (Ramachandran et al., 2016). We showed agreement with previously published results (Joly et al., 2017) that Hrd1 knock-out led to the rescue of Z-A1AT secretion. K8 probably acts at this early step of ERAD, as it is recruited to the Hrd1-Derlin2 complexes. Furthermore, knocking out Hrd1, but not inhibiting p97, led to the rescue of the A1AT secretion. Altogether, these results suggested that reducing K8 expression diminishes ERAD efficacy, increases Z-A1AT maturation and, consequently, enhances Z-A1AT secretion. We postulate that K8 is a novel actor regulating ERAD. Furthermore, retrotranslocation is a crucial checkpoint defining rescuable and non-rescuable forms of misfolded proteins. This limit could be between Derlin2-Hrd1- and p97-governed steps of ERAD degradation when the retro-translocated substrate is undergoing dislocation (**Fig. 7 A and B *vs* C**).

We propose that K8 serves as a scaffolding platform on which other ERAD proteins build up functional complexes (**Fig. 7**). Different phases of retrotranslocation and ubiquitination are highly dynamic and create multiple stable and transient complexes upon stimuli (Eura et al., 2020). Therefore, it is not surprising that K8 can be recruited to many of them (**Fig. 7**) to facilitate transitions and remodelling of these complexes. The precise organisation of the retrotranslocating complexes is still not known. However, the involvement of the Hrd1-Hrd3 (Sel1) complex (Schoebel et al., 2017), Derlin family members (Ye et al., 2004) (Lilley and Ploegh, 2004), and the Hrd1-Der1 complex (Wu et al., 2020) has been shown. Importantly, our results suggest that (i) K8 – Derlin2 complexing is relatively permanent (detected even in mock cells and in cells with reduced K8 expression) and (ii) the recruitment of other ERAD proteins (Hrd1 and Sel1) occurs upon expression of misfolded Z-A1AT.

It could be argued that K8, an abundant protein in epithelial cells, binds non-specifically to intracellular protein complexes. However, as shown by immunocytochemistry, the intracellular distribution of K8 differed between Z-A1AT *vs* WT-A1AT-expressing HeLa and patient-derived HBE cells. It has also been previously observed for patients' derived HBE cells expressing F508del-CFTR or WT-CFTR (Colas et al., 2012b). Moreover, non-specific K8 recruitment to ERAD complexes would be expressed as K8 sedimentation into all fractions in the shK8 cell and in mock-transfected cell lysates, which is not the case.

We postulate that keratins are essential regulators of processes occurring at the endoplasmic reticulum (ER) and Golgi. K18, which forms a heterodimer with K8, also plays a role in F508del-CFTR trafficking (Davezac et al., 2004) by binding to the C-terminus of CFTR while K8 bids to the NBD1 domain (Duan et al., 2012; Colas et al., 2012). Similarly to K8, K18 may be involved at the ER level (Toivola et al., 2010). Importantly, silencing K18 leads to the rescue of F508del-CFTR function (Davezac et al., 2004). On another hand, K18

co-distributes with WT- / Z-A1AT, but the absence of increase of proximity to Z-A1AT in PLA assay (in contrast to K8), suggest that K18 may also be indirectly implicated in ERAD scaffolding. This also reinforces the idea that different rescue mechanisms implicating intermediary filaments exist within ERAD.

Our results are supported by other reports which also indicated that keratins are important proteins regulating processes at the ER and Golgi. K8 specifically binds Hsp70 involved in the ERAD pathway (Liao et al., 1995) (Salas et al., 2016) and K1, belonging to the same family of proteins as K8, forms complexes responsible for the retention of N-acetylglucosaminyltransferase within the Golgi structures (Petrosyan et al., 2015).

A small-molecule c407, which disrupts the interaction between F508del-CFTR and K8 (Odolczyk et al., 2013), and which long-term administration is not toxic in mice (da Cunha et al., 2022) increased Z-A1AT secretion in Z-A1AT-expressing HeLa cells, and importantly, in a more physiological model, differentiated primary HNE cells expressing endogenous Z-A1AT, providing preclinical evidence of potential therapeutic. Because c407 modified K8 and Derlin2 recruitment to ERAD complexes, we propose that K8-Derlin2 complexes represent a potent target for pharmacotherapy. However, c407 treatment did not completely disrupt ERAD complexes because Sel1 and Hrd1 profiles did not change. Such an effect, if it occurred, would be toxic for cells and therefore inappropriate for therapy. Alternatively, the implication of K18 in ERAD scaffolding cannot be excluded. C407 also failed to increase WT-A1AT secretion, contrary to reduced K8 expression, indicative of incompletely overlapping mechanisms of action. Using HDex-MS analysis, we showed that c407 stabilises multiple regions of K8, consistent with direct binding, which may lead to decreased interactions of K8 with other proteins and less efficient formation of protein complexes. Importantly, c407 allowed to restore K8 network which became similar to WT A1AT

expressing cells. HDex-MS experiments on Z-A1AT could not be performed due to its self-polymerisation.

Targeting the early steps of ERAD enables overcoming the difficulties of binding to highly mobile folding intermediates of Z-A1AT (Lomas et al., 2021). One of the early ERAD proteins, Hrd1, has been proposed as a direct therapeutic target for several diseases: rheumatoid arthritis (YAGISHITA et al., 2012) (Rahmati et al., 2018), type 2 diabetes (Wu et al., 2020), Alzheimer's and Parkinson's diseases (Nomura et al., 2016). Pharmacological or genetic inhibition of Hrd1 significantly reduced the severity of rheumatoid arthritis and glucose control in the diabetic model. By contrast, in Alzheimer's and Parkinson's diseases, Hrd1 overexpression leads to suppression of Pael-R- or Aβ1–40 and Aβ1–42-induced cell death (Nomura et al., 2016). Our therapeutical strategy, based on modulation of K8-regulated early ERAD complexes with chemical compounds opens new perspectives for A1ATD and other epithelial protein misfolded diseases (PMDs). The preliminary results obtained in mouse model of nephrotic syndrome due to the mutation in podocin, R138Q, support this hypothesis (Kuzmuk et al., abstract SA-OR-052, Kidney Week 2019). Combining molecules targeting the misfolded protein directly (Lomas et al., 2021) with molecules affecting ERAD (e.g., c407) could lead to enhanced rescue.

In conclusion, we demonstrated that K8 is a scaffolding factor for early-stage ERAD complexes regulating the degradation of ERAD substrates and propose targeting ERAD complexes containing K8 as an attractive strategy for the pharmacotherapy of A1AD and possibly other epithelial PMDs.

Materials and methods

Cell culture

HeLa cells. HeLa cells transiently transfected with pcDNA3-WT-A1AT or Z-A1AT were cultured in Dulbecco's modified eagle medium (DMEM) and were supplemented with 10% v/v fetal calf serum (FCS), 2 mM L-glutamine, 100 μg/ml streptomycin and 100 units/ml penicillin in a humidified incubator at 37°C 5% v/v CO_2. WT-A1AT/Z-A1AT cDNA was kindly provided by Prof. Eric Chevet (University of Bordeaux, France). Western blot (WB) analysis of WT-A1AT and Z-A1AT extracted from transiently transfected HeLa cells revealed that Z-A1AT-expressing cells produced less fully-glycosylated A1AT than cells transfected with WT-A1AT (**Supp. Fig. 9A, upper left panel**) concomitant with reduced secretion, reaching only 25% of WT secretion level (**Supp. Fig. 9A, bottom left panel and quantification**).

We generated HeLa cells that express reduced amounts of K8 using the shRNA approach (shK8 HeLa cells). WB quantification showed that shK8 HeLa cells expressed ~17% of the normal K8 level (**Supp. Fig. 9C and D**).; transient transfection with either WT-A1AT or Z-A1AT did not affect this level (**Supp. Fig. 9C**).

HeLa cell lines stably expressing the IgM heavy chain subunit μ_s under induction with Mifepristone (Mif, 0.5 nM), WT variant and Hrd1KO, were a kind gift from Dr Eelco van Anken (IRCCS Ospedale, San Raffaele, Italy). These cells were cultured in DMEM (Dulbecco's modified eagle medium) and were supplemented with 5% v/v FCS, 100 μg/ml streptomycin and 100 units/ml penicillin in a humidified incubator at 37°C and 5% v/v CO_2.

HeLa cells are derived from simple epithelium cells, the same type of epithelium as respiratory epithelium and hepatocytes. Importantly, they endogenously express Keratin 8 and are easily transfected with plasmids coding for A1AT or with siRNA or transduced with shRNA. Hela cells are a relevant tool to largely explore the mechanisms observed in physiological context using HBE cells.

16HBE WT and F508del cell lines

16HBE WT cells (full name 16HBE14o- Human bronchial epithelial cell line) are human bronchial epithelial cells isolated from bronchial explant of a patient with WT-CFTR, immortalized with SV40 and clone selected. Cells contain only two copies of *CFTR* gene under natural non-modified expression system.

16HBE F508del cell line (16HBEge CFTR F508del – genetically engineered) used in the study was obtained from Cystic Fibrosis Foundation (CFF) (Valley et al., 2019). This cell line was created from 16HBE14o- cells by CRISPR/Cas9 methodology to introduce the F508del mutation in the *CFTR* gene. Similarly to 16HBE14o- cells, 16HBEge CFTR F508del cells have two alleles of *CFTR* gene, but mutated.

16HBE cells are not transfected nor transduced with CFTR gene. CFTR protein expression is obtained from only two copies of a gene under natural promotor.

Primary HBE/HNE cells. The establishment of primary bronchial epithelial cell cultures from PiZZ AATD patients (n = 3) and MM controls (n = 3) matched according to sex, GOLD stage (0 - III), and smoking status has been previously reported (van 't Wout et al. 2014). Cell cultures were re-established from liquid nitrogen stored stocks. Primary nasal epithelial cell cultures from PiZZ AATD patients (n = 2) and MM control (n = 1) were established from fresh nasal brushing (Pranke et al., 2017). In primary human bronchial epithelial (HBE) and human nasal epithelial (HNE) cells derived from Z-homozygous (PiZZ) or WT-homozygous individuals (**Supp. Fig. 9C**), the fraction of secreted A1AT was lower (<50%) in PiZZ cells than in WT cells. In contrast, intracellular levels of Z-A1AT was increased compared to WT-A1AT (compare **Supp. Fig 9C upper and lower panels**).

Silencing K8 expression

K8 expression was silenced in HeLa cells using a stable shRNA (Thermo Scientific) transduced by lentiviral vectors. HeLa cells containing the shRNA construct and parental HeLa cells were transfected with pcDNA3-A1AT WT or A1AT Z. For the growth or secretion assay in Hrd1KO cells, K8 expression was silenced with siRNA (Dharmacon siRNA Reagents) transiently transfected into HeLa cells with DharmaFect Reagent (Dharmacon).

Protein sample preparation for immunoblotting

- **Cell lysis and cell extract preparation**

Cells were first trypsinised and centrifuged at 300 g for 10 min at 4°C, washed on ice with phosphate-buffered saline (PBS) and recentrifuged at 300 g for 10 min at 4°C. The cell pellet was then resuspended in a lysis buffer composed of Tris-HCl pH 7.5, 20 mM, NaCl 50 mM, EDTA 1 mM, NP40 0.5% v/v and a protease inhibitor cocktail (cOmplete Tablets, Roche, 04 693 124 001) and incubated on ice for 30 min. Next, cell lysates were centrifuged at 1500 g for 15 min at 4°C. Supernatants were transferred to a new set of tubes, and the protein concentration was measured with the DC Protein Assay (BioRad, 500-0113, -0114, -0115) according to the manufacturer's protocols.

- **Preparation of the secreted protein**

Cells were grown to 80-90% confluence and then washed three times with PBS to remove serum. Cultures were then kept in the DMEM media containing only penicillin/streptomycin for 24 h or shorter. Media with secreted proteins were collected, centrifuged at 300 g, divided into aliquots and frozen at -80°C. Each sample used for the WB analysis was defrosted once. Samples for mass spectrometry standard protein identification were send to proteomic SFR Necker core facilities (https://fr.sfr-necker.fr/proteomics).

Western blot analysis

For protein detection by WB samples were mixed with a 5X Laemmli sample buffer and heated at 95°C for 5 min, resolved using a 10% w/v acrylamide SDS-PAGE gel and transferred to nitrocellulose membranes. The membranes were then incubated in a blocking buffer (3% w/v BSA (bovine serum albumin) and 3% w/v milk in PBS-0.1% v/v Tween-20) for 1 h. Proteins of interest were immuno-detected with appropriate antibodies (ab) diluted in a 3% w/v BSA blocking buffer for 1 h. K8 was immuno-detected with mouse monoclonal ab (61038, Progen) at a 1:500 dilution, A1AT was immuno-detected using the primary rabbit polyclonal anti-human A1AT ab (A0012, Dako, Agilent) at a 1:1,000 dilution, Derlin2 was detected with mouse monoclonal ab (sc-398573, Santa Cruz Biot Inc.). Sel1 was detected with mouse monoclonal ab (sc-377350, Santa Cruz Biot Inc.), and Hrd1 was detected with rabbit anti-Synoviolin ab (A302-946A—M, Bethyl). Other abs used were: rabbit polyclonal anti-GAPDH (sc-25778, Santa Cruz Biot Inc.) at a 1:500 dilution, mouse anti-Na^+K^+ATPase (ab7671, Abcam) at a 1:1,000 dilution, mouse monoclonal anti-Hsp70 (sc-24, Santa Cruz Biot Inc.) at a 1:1,000 dilution, rabbit anti-*Gaussia* luciferase (E8023, New England Biolabs) at a 1:2,000 dilution, rat monoclonal anti-Grp78 (sc-13539, Santa Cruz Biot Inc.) at a 1:500 dilution and rabbit polyclonal anti-Calreticulin (SPA-600, Stressgen) at a 1:500 dilution. Finally, nitrocellulose membranes were incubated with appropriate secondary antibodies coupled to fluorochromes, as recommended by the manufacturer (Li-Cor, Bad Homburg, Germany). The detection of the WB results was performed with the Odyssey scanner (Li-Cor, Germany). Quantification of the WB was performed using ImageJ software.

Non-secreted (intracellular) WT-A1AT is detected in western blot in form of two bands, corresponding to non-mature – core-glycosylated (ER form) and mature – fully glycosylated protein (Golgi and post-Golgi form). Intracellular Z-A1AT present mainly one band corresponding to non-mature / core-glycosylated protein (ER form) and a slight amount of mature / fully-glycosylated protein (that escaped from degradation and aggregation in the

ER). Secreted (fully glycosylated) WT-A1AT is detected as only one band. Similarly Z-A1AT if it escape the degradation pathway or aggregation in the ER, it passes through the Golgi to be glycosylated and then secreted.

Immunocytochemistry

HeLa and HBE cells were grown on microscopy slides up to low levels of confluence. The cells on the slides were washed twice with PBS and fixed with ice-cold acetone for 5 min. Next, the slides were washed twice with PBS, dried and stored at -20°C if necessary. The cells were then thawed, rehydrated with phosphate-buffered saline with 0.1% v/v Tween-20 (PBS-T) and incubated in blocking solution 3% w/v BSA in PBS-T for 1 h at room temperature (RT). Protein immunodetection was performed with primary abs diluted in blocking solution during overnight incubation at 4°C: rabbit polyclonal ab against alpha-1-antitrypsin (A0012, Dako, Agilent) at a 1:500 dilution, mouse monoclonal ab against K8 (61038, Progen) at a 1:200 dilution, and goat polyclonal ab against Calnexin (Santa Cruz Biot Inc.) at a 1:500 dilution. The primary antibodies against different proteins were incubated simultaneously. Subsequently, the cells were washed four times for 5 min each in PBS-Tween20 0.1% v/v, and nonspecific binding sites were blocked in 5% v/v goat serum (in PBS-Tween20) for 30 min. The cells were then incubated for 45 min at RT with goat secondary IgGs conjugated to Alexa 488 or 594 at a 1:1,000 dilution in 5% v/v goat serum in PBS-T. After five washes for 5 min each, the Vectashield mounting medium containing DAPI (Vector Laboratories, H-1200) was used to mount the cells on microscope slides. Immunocytochemistry on the air–liquid interface cultures of the primary HBE cells was performed, as described previously (Pranke et al. 2017).

Confocal microscopy

Confocal microscopy was performed as described previously (Pranke et al., 2017). Briefly, a Leica TCS SP5 AOBS confocal microscope (Heidelberg, Germany) was used. Multiple optical z-stack images were captured over the cell culture. The images were analysed with ImageJ software (NIH, USA). The co-localisation level was assessed by the ImageJ plug-in JACoP and tools Image calculator and Measure stack. The PLA results were quantified with the Analyze Particles tool and expressed as an average number of fluorescent spots (nfs), minus the average number of negative controls.

Synthetic lethality assay (Growth assay)

HeLa cells overexpressing IgM heavy chain subunits μ_s under Tet-inducible promoter (Bakunts et al. 2017) (Vitale et al. 2019) were kindly provided by Dr Eelco van Anken. In the absence of light chains, heavy chains cannot reconstitute IgM and cannot be secreted. The μ_s is retained in the ER, and its accumulation activates the unfolded protein response. Once the ERAD pathway is deactivated, heavy chains overload the ER leading to synthetic lethality through apoptosis, defining which factors are crucial to act in conjunction with Hrd1 and Sel1L in the disposal of μ_s (Vitale et al., 2019). The experiments were performed according to a previously published protocol (Bakunts et al., 2017). The HeLa cells overexpressing IgM heavy chain subunit μ_s upon induction with 0.5 nM Mifepristone (Mif) were first transfected with siRNA directed against K8 and scrambled sequence (Dharmacon siRNA Reagents). Non-transfected cells and cells 24 h after transfection were trypsinised, counted with a Malassez chamber, and seeded upon 1:5 serial dilutions (5,000, 1,000, and 200 cells per well) in 24-well plates. Mifepristone (0.5 nM) was added after cells were attached to the growth surface. To assess growth differences between tested conditions, cells were grown for 7 days. Culture media and pharmacological agents were refreshed every 2-3 days. Cells were then fixed with methanol-acetone (1:1) for 10 min, stained with 0.5% crystal violet in 20% methanol for 10 min, and washed with distilled water afterwards. Dried plates were imaged

552 with the ChemiDoc TM XRS+ (BioRad). The intensity of crystal violet staining was
553 quantified with ImageJ software (NIH). An average intensity of empty wells on the same plate
554 served for background subtraction. Quantification of growth was presented for wells with a
555 seeding of 1,000 cells.

556 **ERAD complexes fractionation**

557 The experiments were performed as described in (Vitale et al. 2019). HeLa cells were grown
558 on T75 flasks up to 75% of confluence and transfected with plasmids coding for WT-A1AT
559 or Z-A1AT using the Lipofectamine 3000 protocol (Thermo Fisher Scientific). Additionally,
560 heavy chains μ_s were induced with Mifepristone 0.5 nM 24h before harvesting the cells. Cell
561 lysis was performed 48h post-transfection with a lysis buffer (50 mM Tris-HCl pH 7.4, 150
562 mM NaCl, 5 mM EDTA, 1% lauryl maltose neopentyl glycol (LMNG)) containing a mix of
563 proteases inhibitors (cOmplete Tablets, Roche, 04 693 124 001). After centrifugation at 5,000
564 g for 10 min, cell lysates were loaded on the top of 10 % - 40 % linear sucrose gradients and
565 centrifuged at 39,000 rpm / 17 h / 4°C in a SW41Ti rotor. Sucrose gradients were prepared
566 with a Hoefer gradient maker. The 13 fractions were collected from low density at the top of
567 the gradient to high density at the bottom. Proteins were precipitated with trichloroacetic acid
568 and washed with ice-cold acetone. Protein pellets were resuspended in a Laemmli buffer
569 containing dithiotreitol (DTT, 10 mM), heated at 50°C before separation by SDS-PAGE.
570 After protein transfer to nitrocellulose membrane, proteins were detected with appropriate
571 antibodies: K8 – mouse monoclonal ab (61038, Progen), Sel1 (sc-377350, Santa Cruz Biot
572 Inc.), Hrd1/Synoviolin (A302-946A-M, Bethyl), and Derlin2 (sc-398573, Santa Cruz Biot
573 Inc.). The intensity of each protein band was measured using ImageJ (NIH Bethesda) and
574 expressed as % of a sum of all fractions.

575 **Preparation of cell microsomes**

The cells grown in flasks were washed with PBS, trypsinised and centrifuged at 300 g for 5 min at 4°C. The cell pellet was washed twice in PBS, recentrifuged at 300 g for 5 min at 4°C and resuspended in 800 µl of the isotonic extraction buffer (10 mM HEPES, pH 7.8, 250 mM sucrose, 25 mM potassium chloride and 1 mM EDTA) in the presence of a protease inhibitor cocktail (Roche). Cell lysis was performed using mechanical homogenisation with constant incubation of the samples on ice. Up to 70% of the sample showed disrupted cells when observed under microscope. The homogenised cells were then transferred to prechilled 1.5 ml tubes and centrifuged at 6000 g for 10 min at 4°C; the collected supernatant was recentrifuged in a fresh tube at 9000 g for 15 min at 4°C. A new supernatant was collected in a prechilled 1.5 ml ultracentrifuge tube and centrifuged at 100000 g for 1 h at 4°C in a TLA-55 rotor (Beckman Coulter). The resulting pellet was resuspended in the same isotonic buffer containing antiproteases and was frozen at -80°C together with the 100000 g supernatant, which represented the cytosolic fraction.

Co-immunoprecipitation

HeLa cells were grown on 4 T75 culture flasks up to 75-85 % confluence, transfected with WT- or Z-A1AT, and collected by trypsinisation 48h after transfection. 16HBE cells were grown on 4 T75 flasks and maintained in 100% confluence for 3-4 days, and trypsinised. Polarized primary HNE cells were grown and differentiated on microporous filters for 3 weeks, washed twice with PBS and collected directly before cell lysis by scraping in isotonic lysis buffer. The cell pellets (HeLa and 16HBE cells) were washed twice with PBS and then resuspended in isotonic lysis buffer (see protocol Preparation of microsomes) with addition of protease inhibitor cocktail (Roche) and homogenized on ice with mechanic homogenizer. Cell lysates were then sequentially centrifuged as described in protocol Preparation of microsomes to obtain microsomes pellet. The resulting pellet was resuspended in lysis buffer containing LMNG detergent (see protocol ERAD complexes fractionation) containing a mix of proteases inhibitors. Next, Dynabeads Protein G beads were washed twice with PBS-Tween20 0.01% v/v and incubated with an antibody solution (1 µg / 20 µl of beads) containing

anti-Derlin2 antibody (sc-398573, Santa Cruz Biot Inc.) or anti-K8 (ref 61038, Progen, Germany) for 1 h at RT with constant rotation. A negative control with mouse IgG (ref 12-371, Merck-Millipore) was prepared using the same protocol. The beads were washed with PBS-Tween20 0.01% v/v, and a DSS crosslinker was added at a final concentration of 100 μM for 15 min, which then was quenched by addition of Tris-HCl pH 7.5. The beads with the crosslinked antibody were mixed with cell lysates and incubated for 2 h at 4°C at a constant rotation. After incubation, cell lysates were removed, and the beads were washed three times with LMNG lysis buffer (containing 1.5% of LMNG); the immuno-precipitated proteins were eluted with a Laemmli sample buffer at 37°C for 15 min.

Proteinase K assay on the microsomal fraction

The Proteinase K assay, as adapted from Besingi and Clark (2015), was designed to detect the presence or absence of a K8 protein in the interior of the ER/microsomal compartment or at the cytosolic periphery of the ER membrane. HeLa cells transfected with cDNA A1AT were grown in a T150 culture flask, trypsinised, washed with PBS and pelleted at 300 g for 5 min at 4°C. The microsomal fraction was purified, as described in the section 'Cell microsomes preparation'. The microsomes were resuspended in the isotonic buffer. Each of the samples containing the microsomes was divided into two volumes. The first half of the microsomes was diluted in the same isotonic buffer, and the second was diluted in the isotonic buffer containing 1% v/v Triton X-100 (final Triton X-100 concentration 0.5% v/v) and incubated for 15 min to solubilise membranes and release intramicrosomal proteins. Next, the two samples (with and without Triton X-100) were divided to retain a nondigested aliquot; Proteinase K was added to the second aliquot to a working concentration of 125 μg/ml. It is assumed that Proteinase K digests all proteins in Triton X-100-treated samples and only externally/transmembrane-located proteins in nontreated samples. All samples – (i) microsomes in isotonic buffer; (ii) microsomes in isotonic buff. + Proteinase K; (iii) microsomes + Triton X-100; (iv) microsomes + Triton X-100 + Proteinase K – were

incubated at 37°C for 20 min. All samples were resolved on 10% SDS-PAGE gels and immunoblotted to detect A1AT (Dako, Agilent), K8 (Progen, Germany), Calreticulin (Stressgen) and Na^+K^+ATPase (Abcam).

Proximity ligation assay

Cells were grown on microscopy cover slips up to 50–60% confluence. The cells were washed twice with PBS and fixed with ice-cold acetone for 5 min. Afterwards, the slides were washed twice with PBS and dried before being stored at -20°C. The PLA experiments were performed according to the manufacturer's instructions (Olink). First, the cells were humidified with PBS-Tween 20 0.1% v/v and incubated in a blocking solution provided with the kit for 30 min at 37°C. Next, the two primary anti-K8 mouse monoclonal (Progen) and anti-A1AT rabbit polyclonal (Dako) antibodies were diluted in dilution buffer (Olink) for 1 h at 37°C. After three washes with TBS-Tween 20 0.1% v/v, the cells were incubated with the PLA probes (secondary abs provided by Olink) specific to primary mouse and rabbit IgGs and were coupled with the oligonucleotides for 1 h at 37°C. The cells were then washed three times with TBS-T and incubated with a ligation mixture composed of the ligase and oligonucleotide-connectors (sequences homologous to the oligonucleotides conjugated with PLA probes). Connectors can hybridise with PLA probes only when the distance between the proteins is < 40 nm and then will form an enzymatically ligated circle. In the next step, after washing with TBS-T, the polymerization mixture with polymerase and nucleotides coupled with fluorochromes were added for amplification of the circular oligonucleotides as a template, using the PLA probe sequences as primers. Cells were mounted on microscopy slides with a Vectashield mounting medium containing DAPI. The negative controls were prepared using an identical procedure but by applying only one of the primary antibodies. Included positive control presents interaction between A1AT and Calnexin.

Cell culture treatments

652 HeLa cells treatments with the VCP/p97 inhibitor Eeyarestatine I (10 μM, Sigma Aldrich) in
653 DMSO were done for 8 h, and NMS-873 (1μM, Selleckchem) in DMSO for 20 h, at 37°C in
654 the CO_2 incubator. HeLa cells were treated with 5μg/ml Brefeldin A for 7 h at 37°C in the
655 CO_2 incubator. Mifepristone was used at concentration of 0.5 nM for 6 days in the growth
656 assay or for 48 h for secretion assay. Corrector molecule c407 was tested at final
657 concentrations of 1, 5, 10, 20, and 35 μM. Wortmannin (1 μM) and MK-2206 (5 μM) for 20 h
658 treatment of HeLa cells.

659 **HDX-MS workflow and analysis**

660 The HDX-MS experiments were performed as described previously (52), but with some minor
661 modifications. Briefly, the undeuterated and deuterated WT-A1AT samples in their unbound and
662 bound states were digested online using a 2.1 mm × 30 mm immobilised pepsin resin column
663 (Porozyme, ABI, Foster City, CA) with 0.07% v/v formic acid in water as the mobile phase (200
664 μl/min flow rate). The peptides were passed directly to the 2.1 mm × 5 mm C18 trapping column
665 (ACQUITY BEH C18 VanGuard precolumn, 1.7 μm resin; Waters, Milford, MA). The trapped
666 peptides were eluted onto a reversed phase column (Acquity UPLC BEH C18 column, 1.0 × 100 mm,
667 1.7 μm resin, Waters, Milford, MA) using an 8–40% gradient of acetonitrile in 0.1% v/v formic acid at
668 90 μl/min, which was controlled by the nanoACQUITY Binary Solvent Manager. The total time of a
669 single run was 13.5 min. All fluidics, valves and columns, except for the pepsin digestion column,
670 were maintained at 0.5 °C by using the HDX Manager (Waters, Milford, MA). The C18 column outlet
671 was coupled directly with the ion source of the SYNAPT G2 HDMS mass spectrometer (Waters,
672 Milford, MA) while working in the ion mobility mode. Lock mass was activated and carried out using
673 Leucine–enkephalin (Sigma). For protein identification, the mass spectra were acquired in the MSE
674 mode over a m/z range of 50–2000. The spectrometer parameters were as follows: ESI-positive mode,
675 capillary voltage 3 kV, sampling cone voltage 35 V, extraction cone voltage 3 V, source temperature
676 80°C, desolvation temperature 175°C and desolvation gas flow 800 L/h. The spectrometer was
677 calibrated using standard calibrating solutions. Peptides were identified using the ProteinLynx Global
678 Server software (PLGS, Waters, Milford, MA). The list of identified peptides containing peptide m/z,

charge, retention time and ion mobility/drift time was passed to the DynamX 3.0 data analysis programme (Waters, Milford, MA). The average masses of the peptides in the exchange experiment (Mex) at different incubation times (0s (M_ex^0) – 10 s, 1 min, 5 min, 30 min, 150 min and 1440 min (M_ex^MAX)) – obtained from the automated analysis were then verified by visual inspection. Ambiguous or overlapping isotopic envelopes were discarded from further analysis. The fraction of deuterium exchanged by a given peptide was calculated according to equation 1 (Eq. 1), as follows:

$$Eq.1 - \ Fraction\ Exchanged = \frac{M_{ex} - \mathrm{M}_{ex}^{0}}{\mathrm{M}_{ex}^{MAX} - \mathrm{M}_{ex}^{0}}$$

Error bars for the difference in deuteration were calculated as the standard deviations of three independent experiments. A student's t-test for two independent samples with unequal variances and unequal sample sizes (also known as Welch's t-test) was carried out to evaluate the differences in fractions exchanged between the same peptides in two different states. The final figures were plotted either using OriginPro 8.0 (OriginLab) software or R-project for Statistical Computing.

Statistics

The experiments were repeated at least three times. The results are expressed as mean ± SD and analysed using Mann-Whitney test or as described for specific experiments.

Declarations

Ethics approval and consent to participate

This study was performed in line with the principles of the Declaration of Helsinki. Approval was granted by the Ethics Committee of Ile-de-France 2 (CPP IDF2: 2010-05-03-3).

Written informed consent was obtained from all individual participants included in the study or parents of children under 16.

Consent to publish

Not applicable.

Availability of data and material

The datasets generated during and/or analysed during the current study are available from the corresponding author on reasonable request.

Competing Interests

The authors have no relevant financial or non-financial interests to disclose.

Funding

This work was supported by Agence Nationale de la Recherche (ANR-13-BSV1-0019-01, and ANR-18-CE14-0004) and Chancellerie des universites de Paris (legs Poix, 15LEG005_9UMS1151).

Acknowledgements

The authors thank Dr. Eric Chevet for A1AT/Z-A1AT plasmids, Annemarie van Schadewijk for help in culturing the HBE cells, and Anush Bakhunts for μ_s expressing HeLa cells. We thank Dr Grazyna Faure, Dr. Stefano Fumagali and Dr Olivier Namy for helpful discussions and advices. We thank Muriel Girard and Dominique Debray for providing the A1AT/Z-A1AT primary cells and Prof. Hideki Nishitoh for HEK Derlin1/2 KO cells. We thank Dr Chiara Guerrera and Dr Joanna Lipecka from Proteomic SFR Necker core facility for protein identifications. We are very grateful to Isabelle Hatin for technical assistance, and the cell imaging platform for assistance with microscopy experiments.

Authors' contributions:

Iwona Maria Pranke participated in the experimental strategy preparation, conceived the protocols, performed experiments, analysed and interpreted results and wrote the manuscript; Benoit Chevalier performed biochemistry experiments; Aiswarya Premchandar performed mass spectrometry experiments and analysis; Nesrine Baatallah and Kamil F. Tomaszewski

performed some biochemistry experiments; Sara Bitam established the shRNAK8 cell line; Danielle Tondelier performed cell biology experiments; Anita Golec participated in primary cell culture and biochemistry experiments; Jan Stolk provided the A1AT/Z-A1AT primary cells; Gergely L. Lukacs participated in the experimental strategy preparation; Pieter S Hiemstra, Michal Dadlez and David A Lomas participated in the writing of the manuscript; James A Irving participated in preparing the experimental strategy and edited the manuscript; Agnes Delaunay-Moisan participated in designing the experimental strategy and editing of the manuscript; Eelco van Anken participated in preparing the experimental strategy; Alexandre Hinzpeter performed cell biology experiments and wrote the manuscript; Isabelle Sermet-Gaudelus participated in preparing the experimental strategy and writing of the manuscript; Aleksander Edelman conceived of and coordinated the project and wrote the manuscript. All authors reviewed the manuscript and approved its submission.

Author comments

This data has been published on a pre-print server bioRXiv ('https://www.biorxiv.org/content/10.1101/2022.02.01.478623v1').

References

Bakunts A, Orsi A, Vitale M, et al (2017) Ratiometric sensing of BiP-client versus BiP levels by the unfolded protein response determines its signaling amplitude. eLife 6:e27518. https://doi.org/10.7554/eLife.27518

Baldridge RD, Rapoport TA (2016) Autoubiquitination of the Hrd1 Ligase Triggers Protein Retrotranslocation in ERAD. Cell 166:394–407. https://doi.org/10.1016/j.cell.2016.05.048

Besingi RN, Clark PL (2015) Extracellular Protease Digestion to Evaluate Membrane Protein Cell Surface Localization. Nat Protoc 10:2074–2080. https://doi.org/10.1038/nprot.2015.131

Carlson EJ, Pitonzo D, Skach WR (2006) p97 functions as an auxiliary factor to facilitate TM domain extraction during CFTR ER-associated degradation. EMBO J 25:4557–4566. https://doi.org/10.1038/sj.emboj.7601307

Chakraborty P, Teckman J (2014) Alpha-1- Antitrypsin Deficiency Liver Disease: Science and Therapeutic Potential 50 Years Later. J Gastroenterol Pancreatol Liver Disord 1:

Christianson JC, Ye Y (2014) Cleaning up in the endoplasmic reticulum: ubiquitin in charge. Nat Struct Mol Biol 21:325–335. https://doi.org/10.1038/nsmb.2793

Colas J, Faure G, Saussereau E, et al (2012) Disruption of cytokeratin-8 interaction with F508del-CFTR corrects its functional defect. Hum Mol Genet 21:623–634. https://doi.org/10.1093/hmg/ddr496

Coulombe PA, Omary MB (2002) "Hard" and "soft" principles defining the structure, function and regulation of keratin intermediate filaments. Curr Opin Cell Biol 14:110–122. https://doi.org/10.1016/s0955-0674(01)00301-5

Coulombe PA, Wong P (2004) Cytoplasmic intermediate filaments revealed as dynamic and multipurpose scaffolds. Nat Cell Biol 6:699–706. https://doi.org/10.1038/ncb0804-699

da Cunha MF, Pranke I, Sassi A, et al. (2022) Systemic bis-phosphinic acid derivative restores chloride transport in Cystic Fibrosis mice. Sci Rep. 12(1):6132. doi: 10.1038/s41598-022-09678-9.

Davezac N, Tondelier D, Lipecka J, et al (2004) Global proteomic approach unmasks involvement of keratins 8 and 18 in the delivery of cystic fibrosis transmembrane conductance regulator (CFTR)/deltaF508-CFTR to the plasma membrane. Proteomics 4:3833–3844. https://doi.org/10.1002/pmic.200400850

Dong X-M, Liu E-D, Meng Y-X, et al (2016) Keratin 8 limits TLR-triggered inflammatory responses through inhibiting TRAF6 polyubiquitination. Sci Rep 6:32710. https://doi.org/10.1038/srep32710

Duan Y, Sun Y, Zhang F, et al (2012) Keratin K18 increases cystic fibrosis transmembrane conductance regulator (CFTR) surface expression by binding to its C-terminal hydrophobic patch. J Biol Chem. 287(48):40547-59. doi: 10.1074/jbc.M112.403584.

El Khouri E, Le Pavec G, Toledano MB, Delaunay-Moisan A (2013) RNF185 is a novel E3 ligase of endoplasmic reticulum-associated degradation (ERAD) that targets cystic fibrosis transmembrane conductance regulator (CFTR). J Biol Chem 288:31177–31191. https://doi.org/10.1074/jbc.M113.470500

Eura Y, Miyata T, Kokame K (2020) Derlin-3 Is Required for Changes in ERAD Complex Formation under ER Stress. Int J Mol Sci 21:6146. https://doi.org/10.3390/ijms21176146

Ghouse R, Chu A, Wang Y, Perlmutter DH (2014) Mysteries of α1-antitrypsin deficiency: emerging therapeutic strategies for a challenging disease. Dis Model Mech 7:411–419. https://doi.org/10.1242/dmm.014092

Glenn KA, Wen H, Dankle G (2012) Lectin–Like Ubiquitin Ligases Degrade Alpha-1 Antitrypsin-Z. FASEB J 26:lb112–lb112

Graham KS, Le A, Sifers RN (1990) Accumulation of the insoluble PiZ variant of human alpha 1-antitrypsin within the hepatic endoplasmic reticulum does not elevate the steady-state level of grp78/BiP. J Biol Chem 265:20463–20468

Herrmann H, Aebi U (2004) Intermediate filaments: molecular structure, assembly mechanism, and integration into functionally distinct intracellular Scaffolds. Annu Rev Biochem 73:749–789. https://doi.org/10.1146/annurev.biochem.73.011303.073823

Jensen TJ, Loo MA, Pind S, et al (1995) Multiple proteolytic systems, including the proteasome, contribute to CFTR processing. Cell 83:129–135. https://doi.org/10.1016/0092-8674(95)90241-4

Joly P, Vignaud H, Martino JD, et al (2017) ERAD defects and the HFE-H63D variant are associated with increased risk of liver damages in Alpha 1-Antitrypsin Deficiency. PLOS ONE 12:e0179369. https://doi.org/10.1371/journal.pone.0179369

Kerem B, Rommens JM, Buchanan JA, et al. (1989) Identification of the cystic fibrosis gene: genetic analysis. Science. 245(4922):1073–1080. http://dx.doi.org/10.1126/science.2570460

Khodayari N, Marek G, Lu Y, et al (2017a) Erdj3 has an essential role for Z variant Alpha-1-Antitrypsin Degradation. J Cell Biochem. https://doi.org/10.1002/jcb.26069

Khodayari N, Wang RL, Marek G, et al (2017b) SVIP regulates Z variant alpha-1 antitrypsin retro-translocation by inhibiting ubiquitin ligase gp78. PloS One 12:e0172983. https://doi.org/10.1371/journal.pone.0172983

Kim S, Skach W (2012) Mechanisms of CFTR Folding at the Endoplasmic Reticulum. Front Pharmacol 3:201. https://doi.org/10.3389/fphar.2012.00201

Kroeger H, Miranda E, MacLeod I, et al (2009) Endoplasmic reticulum-associated degradation (ERAD) and autophagy cooperate to degrade polymerogenic mutant serpins. J Biol Chem 284:22793–22802. https://doi.org/10.1074/jbc.M109.027102

Lim Y, Kim S, Yoon HN, Ku NO. (2021) Keratin 8/18 Regulate the Akt Signaling Pathway. Int J Mol Sci 22(17):9227. doi: 10.3390/ijms22179227.

Lomas DA, Evans DL, Finch JT, Carrell RW (1992) The mechanism of Z alpha 1-antitrypsin accumulation in the liver. Nature 357:605–607. https://doi.org/10.1038/357605a0

Lomas DA, Irving JA, Arico-Muendel C, et al (2021) Development of a small molecule that corrects misfolding and increases secretion of Z α1 -antitrypsin. EMBO Mol Med 13:e13167. https://doi.org/10.15252/emmm.202013167

Mashukova A, Forteza R, Salas PJ (2016) Functional analysis of keratin-associated proteins in intestinal epithelia: heat-shock protein chaperoning and kinase rescue. Methods Enzymol 569:139–154. https://doi.org/10.1016/bs.mie.2015.08.019

Mehrtash AB, Hochstrasser M (2019) Ubiquitin-dependent protein degradation at the endoplasmic reticulum and nuclear envelope. Semin Cell Dev Biol 93:111–124. https://doi.org/10.1016/j.semcdb.2018.09.013

828 Nomura J, Hosoi T, Kaneko M, et al (2016) Neuroprotection by Endoplasmic Reticulum
829 Stress-Induced HRD1 and Chaperones: Possible Therapeutic Targets for Alzheimer's
830 and Parkinson's Disease. Med Sci 4:14. https://doi.org/10.3390/medsci4030014

831 Odolczyk N, Fritsch J, Norez C, et al (2013) Discovery of novel potent ΔF508-CFTR
832 correctors that target the nucleotide binding domain. EMBO Mol Med 5:1484–1501.
833 https://doi.org/10.1002/emmm.201302699

834 Okiyoneda T, Lukacs GL (2012) Fixing cystic fibrosis by correcting CFTR domain assembly.
835 J Cell Biol 199:199–204. https://doi.org/10.1083/jcb.201208083

836 Okiyoneda T, Veit G, Dekkers JF, et al (2013) Mechanism-based corrector combination
837 restores ΔF508-CFTR folding and function. Nat Chem Biol 9:444–454.
838 https://doi.org/10.1038/nchembio.1253

839 Perlmutter DH (2006) The role of autophagy in alpha-1-antitrypsin deficiency: a specific
840 cellular response in genetic diseases associated with aggregation-prone proteins.
841 Autophagy 2:258–263

842 Pranke IM, Hatton A, Simonin J, et al (2017) Correction of CFTR function in nasal epithelial
843 cells from cystic fibrosis patients predicts improvement of respiratory function by
844 CFTR modulators. Sci Rep 7:7375. https://doi.org/10.1038/s41598-017-07504-1

845 Premchandar A, Kupniewska A, Tarnowski K, et al (2015) Analysis of distinct molecular
846 assembly complexes of keratin K8 and K18 by hydrogen-deuterium exchange. J Struct
847 Biol 192:426–440. https://doi.org/10.1016/j.jsb.2015.10.001

848 Rahmati M, Moosavi MA, McDermott MF (2018) ER Stress: A Therapeutic Target in
849 Rheumatoid Arthritis? Trends Pharmacol Sci 39:610–623.
850 https://doi.org/10.1016/j.tips.2018.03.010

851 Ruggiano A, Foresti O, Carvalho P (2014) ER-associated degradation: Protein quality control
852 and beyond. J Cell Biol 204:869–879. https://doi.org/10.1083/jcb.201312042

853 Schmidt BZ, Perlmutter DH (2005) Grp78, Grp94, and Grp170 interact with alpha1-
854 antitrypsin mutants that are retained in the endoplasmic reticulum. Am J Physiol
855 Gastrointest Liver Physiol 289:G444-455. https://doi.org/10.1152/ajpgi.00237.2004

856 Shen Y, Ballar P, Fang S (2006) Ubiquitin ligase gp78 increases solubility and facilitates
857 degradation of the Z variant of alpha-1-antitrypsin. Biochem Biophys Res Commun
858 349:1285–1293. https://doi.org/10.1016/j.bbrc.2006.08.173

859 Stein A, Ruggiano A, Carvalho P, Rapoport TA (2014) Key steps in ERAD of luminal ER
860 proteins reconstituted with purified components. Cell 158:1375–1388.
861 https://doi.org/10.1016/j.cell.2014.07.050

862 Teckman JH, Burrows J, Hidvegi T, et al (2001) The proteasome participates in degradation
863 of mutant alpha 1-antitrypsin Z in the endoplasmic reticulum of hepatoma-derived
864 hepatocytes. J Biol Chem 276:44865–44872. https://doi.org/10.1074/jbc.M103703200

Toivola DM, Krishnan S, Binder HJ, et al (2004) Keratins modulate colonocyte electrolyte transport via protein mistargeting. J Cell Biol 164:911–921. https://doi.org/10.1083/jcb.200308103

Toivola DM, Strnad P, Habtezion A, Omary MB (2010) Intermediate filaments take the heat as stress proteins. Trends Cell Biol 20:79–91. https://doi.org/10.1016/j.tcb.2009.11.004

Valley HC, Bukis KM, Bell A, Cheng Y, Wong E, Jordan NJ, Allaire NE, Sivachenko A, Liang F, Bihler H, Thomas PJ, Mahiou J, Mense M. Isogenic cell models of cystic fibrosis-causing variants in natively expressing pulmonary epithelial cells. J Cyst Fibros. 2019 Jul;18(4):476-483. doi: 10.1016/j.jcf.2018.12.001. Epub 2018 Dec 15. PMID: 30563749.

van 't Wout EFA, Dickens JA, van Schadewijk A, et al (2014) Increased ERK signalling promotes inflammatory signalling in primary airway epithelial cells expressing Z α1-antitrypsin. Hum Mol Genet 23:929–941. https://doi.org/10.1093/hmg/ddt487

Varga K, Jurkuvenaite A, Wakefield J, et al (2004) Efficient intracellular processing of the endogenous cystic fibrosis transmembrane conductance regulator in epithelial cell lines. J Biol Chem 279:22578–22584. https://doi.org/10.1074/jbc.M401522200

Vasic V, Denkert N, Schmidt CC, et al (2020) Hrd1 forms the retrotranslocation pore regulated by auto-ubiquitination and binding of misfolded proteins. Nat Cell Biol 22:274–281. https://doi.org/10.1038/s41556-020-0473-4

Vitale M, Bakunts A, Orsi A, et al (2019) Inadequate BiP availability defines endoplasmic reticulum stress. eLife 8:. https://doi.org/10.7554/eLife.41168

Wu T, Zhang S, Xu J, et al (2020) HRD1, an Important Player in Pancreatic β-Cell Failure and Therapeutic Target for Type 2 Diabetic Mice. Diabetes 69:940–953. https://doi.org/10.2337/db19-1060

YAGISHITA N, ARATANI S, LEACH C, et al (2012) RING-finger type E3 ubiquitin ligase inhibitors as novel candidates for the treatment of rheumatoid arthritis. Int J Mol Med 30:1281–1286. https://doi.org/10.3892/ijmm.2012.1129

Figures and Figure legend

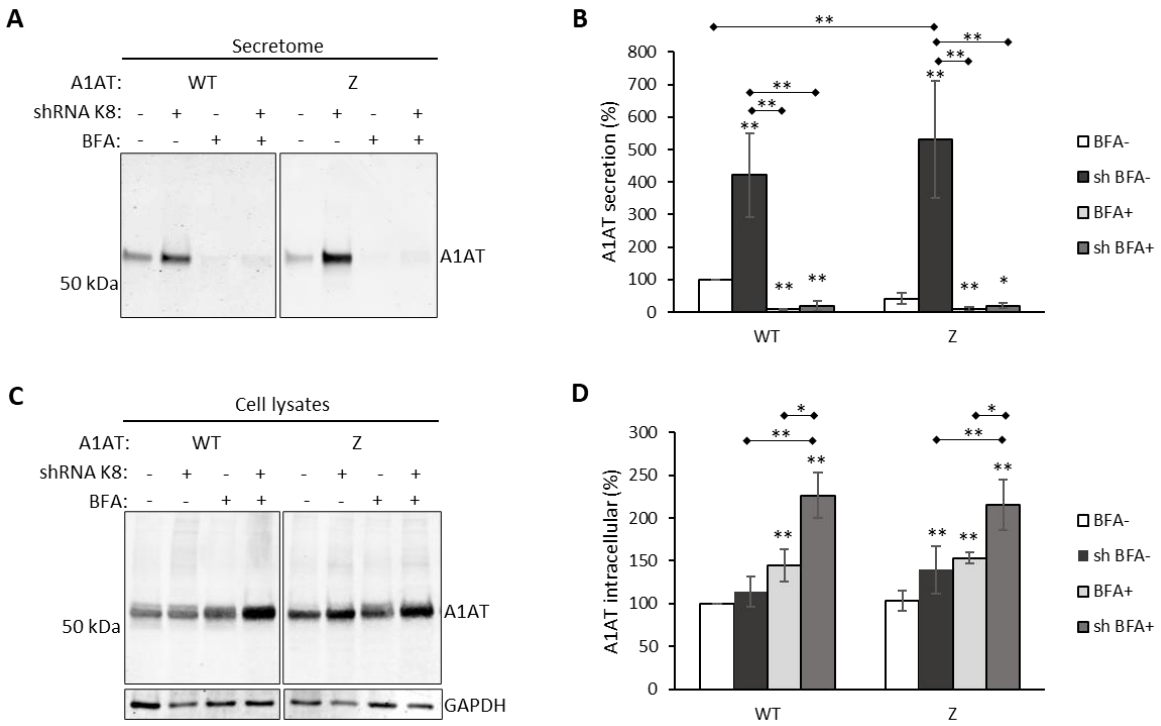

894

895 **Figure 1.** Silencing K8 in HeLa cells increases the secretion of Z-A1AT and WT-A1AT
896 through conventional secretory pathway.

897 **(A)** WB analysis of secretion of WT-A1AT/Z-A1AT in cell cultures with normal
898 (shRNAK8-) and decreased (shRNAK8+) level of K8 expression after treatment
899 with Brefeldin A 5µg/ml (BFA+) or vehicle (BFA-) for 7 hours. Representative
900 image and quantification from n=9 independent experiments.

901 **(B)** Quantification of secretion (mean±SD) normalised to total protein concentrations in
902 respective cell lysates from at least four experiments. * < 0.05; ** < 0.005; *** <
903 0.0005 (Mann-Whitney test); * over the bar indicates p value vs. control (white
904 boxes), if otherwise it is indicated.

905 **(C)** WB analysis of intracellular WT-A1AT/Z-A1AT in cell cultures with normal
906 (shRNAK8-) and decreased (shRNAK8+) level of K8 expression after treatment
907 with Brefeldin A 5µg/ml (BFA+) or vehicle (BFA-) for 7 hours. Representative
908 image and quantification from n=9 independent experiments.

(D) Quantification of secretion (mean±SD) normalized to total protein concentrations in respective cell lysates from at least 4 experiments. * < 0.05; ** < 0.005; *** < 0.0005 (Mann-Whitney test); * over the bar indicates p value vs. control (white boxes), if otherwise it is indicated.

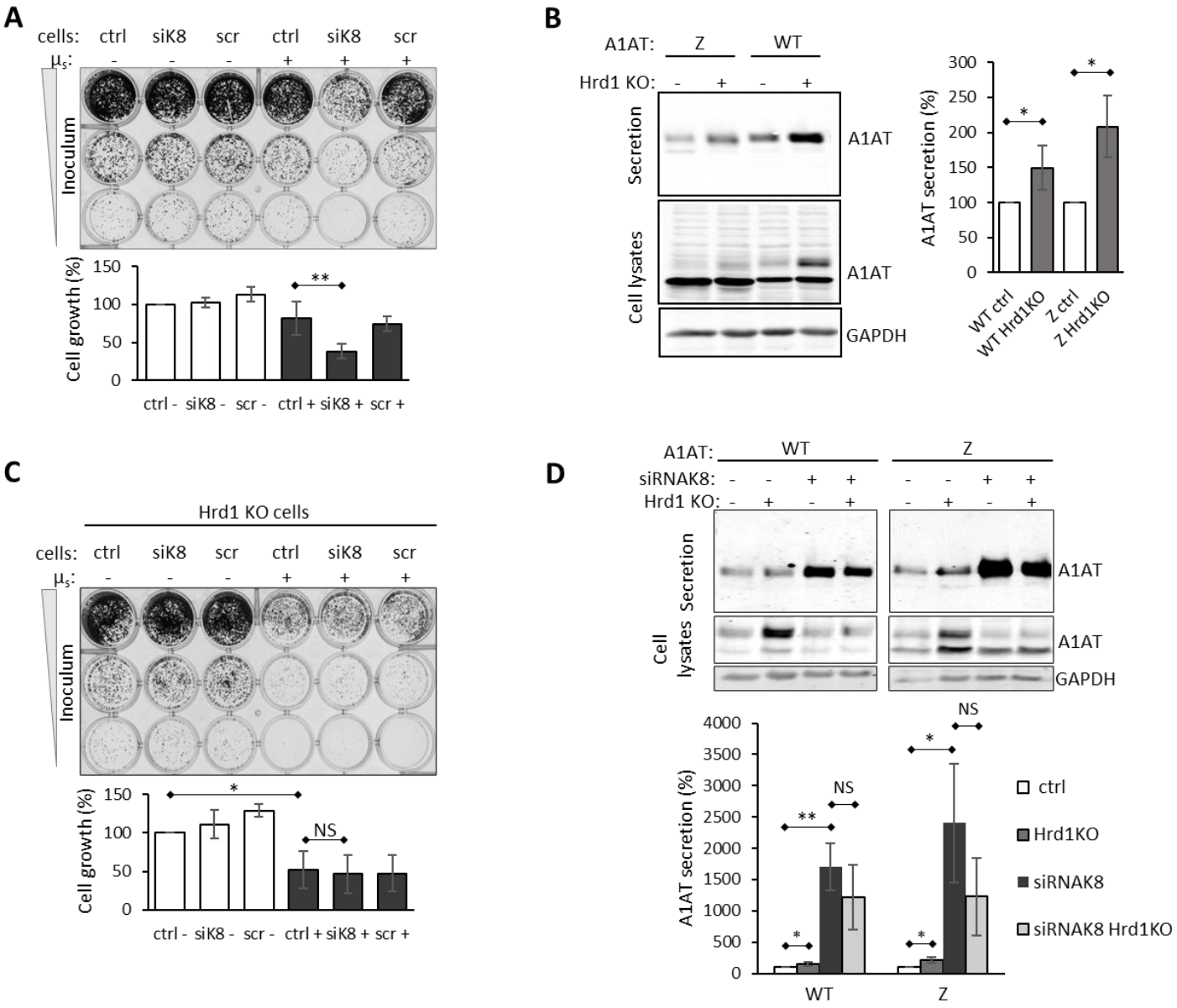
A
cells: ctrl siK8 scr ctrl siK8 scr
μs: - - - + + +
Inoculum
Cell growth (%)
150
100
50
0
**
ctrl - siK8 - scr - ctrl + siK8 + scr +
B
A1AT: Z WT
Hrd1 KO: - + - +
Secretion
Cell lysates
A1AT
A1AT
GAPDH
A1AT secretion (%)
300
250
200
150
100
50
0
*
*
WT ctrl
WT Hrd1KO
Z ctrl
Z Hrd1KO
C
Hrd1 KO cells
cells: ctrl siK8 scr ctrl siK8 scr
μs: - - - + + +
Inoculum
Cell growth (%)
150
100
50
0
*
NS
ctrl - siK8 - scr - ctrl + siK8 + scr +
D
A1AT: WT Z
siRNAK8: - - + + - - + +
Hrd1 KO: - + - + - + - +
Secretion
Cell lysates
A1AT
A1AT
GAPDH
A1AT secretion (%)
4000
3500
3000
2500
2000
1500
1000
500
0
NS
*
NS
**
*
*
ctrl
Hrd1KO
siRNAK8
siRNAK8 Hrd1KO
WT
Z

Figure 2. K8 regulates Hrd1-dependent processes

(A) Synthetic lethality of HeLa cells conditionally expressing μ_s. Cells transfected with siRNA against K8 (cells siK8), or scrambled siRNA (cells scr) were treated with 0.5 nM Mifepristone (Mif) (μ_s+) or vehicle (μ_s-). After transfection cells were seeded upon 1:5 serial dilution (inoculum 5,000, 1,000, 200 cells) into 24-well plates and grown for 7 days. Scrambled RNA had no effect on cell growth of non-expressing (scr-μ_s) and μ_s-expressing cells (scr+μ_s). This is a representative image of a culture plate and quantification of cell growth (inoculum 1,000 cells, middle row) as mean % (±SD) of growth in non-transfected non-treated cells (ctrl-) of five independent experiments are shown. ** $p < 0.005$ (paired t test).

(B) Effect of Hrd1 knock-out on WT-A1AT and Z-A1AT secretion from HeLa cells. WB images show WT-A1AT and Z-A1AT secretion levels (upper panel), A1AT expression (middle panel) and GAPDH as loading control (lower panel). Protein quantification is expressed as means ±SD from four independent experiments. * $p < 0.05$ (Mann-Whitney test).

(C) Synthetic lethality of Hrd1KO HeLa cells. Cells were treated as in Fig. 2A. Representative image of culture plate and quantification of cell growth (inoculum 1,000 cells, middle row) as mean % (± SD) of growth in non-transfected non-treated cells (ctrl-) of five independent experiments are shown. * $p < 0.05$ (paired t test).

(D) Effects of K8 silencing, Hrd1 knock-out and their combination on secretion of WT-A1AT and Z-A1AT. Normal (Hrd1KO-) and Hrd1KO (Hrd1KO+) HeLa cells were transiently transfected with WT-A1AT or Z-A1AT and with siRNA against K8 (siRNAK8+). Representative WB images demonstrating WT-A1AT and Z-A1AT secretion (upper image), WT-A1AT and Z-A1AT expression (middle image) and GAPDH (bottom image) from normal, Hrd1KO+, siRNAK8+ and

siRNAK8+/Hrd1KO+ HeLa cells. Protein quantification of A1AT secretion is expressed as mean ± SD for three experiments. * $p < 0.05$, ** $p < 0.005$ (Mann-Whitney test).

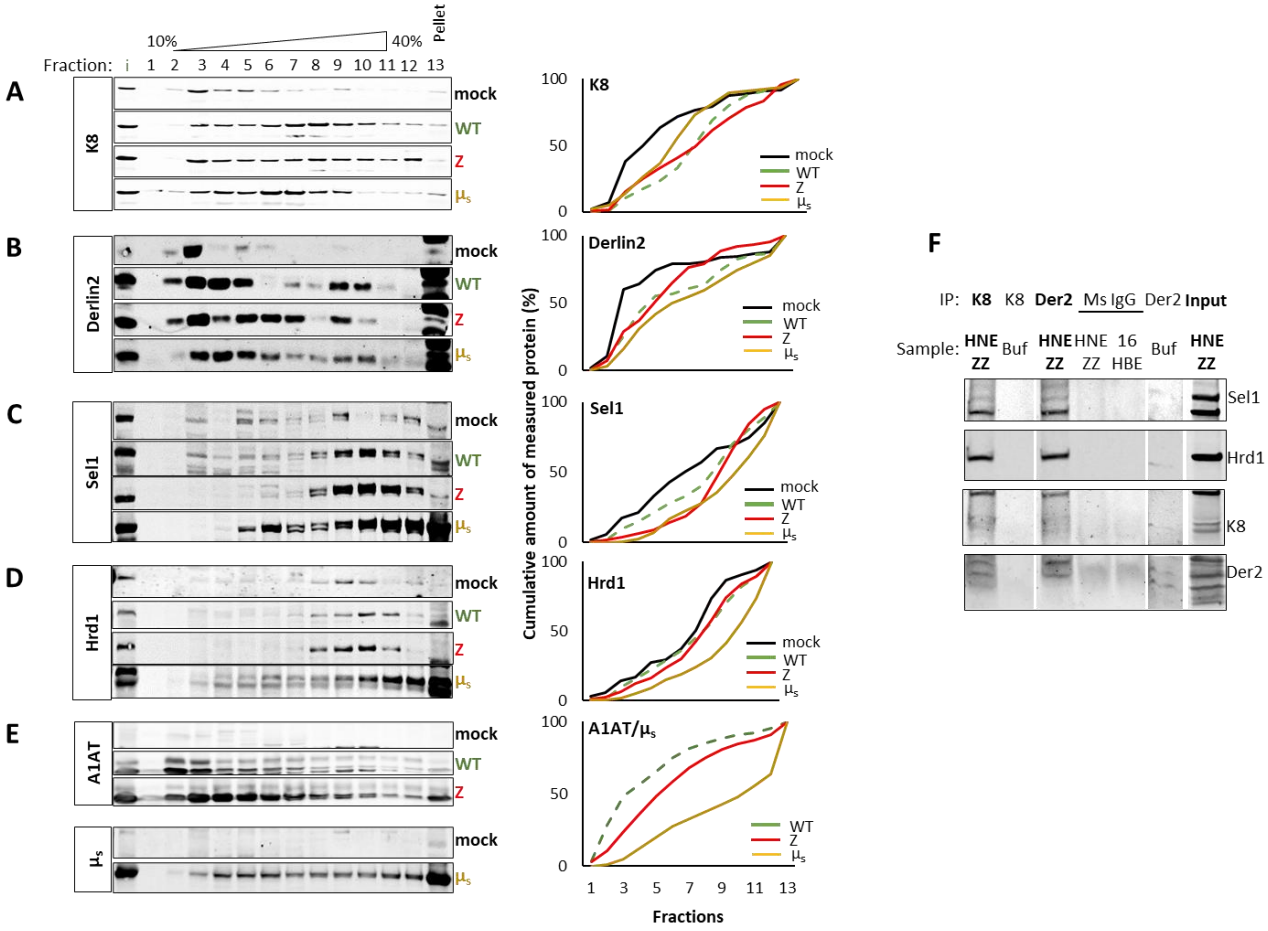

959

960 **Figure 3.** K8 is recruited to the ERAD complexes upon overexpression of misfolded Z-
961 A1AT, WT-A1AT and μ_s.

962 Sucrose gradient fractionation of the ERAD complexes. HeLa cells expressing WT-
963 A1AT (WT-A1AT), Z-A1AT (Z-A1AT), μ_s (Mif 0.5 nM for 24 h) (μs), or mock-
964 transfected (mock). Protein samples from cells were sedimented over a 10–40%
965 sucrose gradient. K8 (A), Sel1 (B), Hrd1 (C), Derlin-2 (D), and μ_s/WT-A1AT/Z-
966 A1AT (E) were detected by immunoblotting with respective antibodies and semi-
967 quantified (right panels). Quantifications represent results shown in the corresponding
968 images on the left and are expressed as cumulative amount of measured protein (%) to
969 demonstrate the overall shift. In the right panel: black lines correspond to protein
970 content in low density ERAD complexes under basal conditions, green, red, and
971 yellow lines show ERAD complexes formed upon WT-A1AT, Z-A1AT and μ_s

expression, respectively. The three tested substrates distributed differently in sucrose gradients: a large amount of μ_s which is a substrate efficiently processed by ERAD strongly distributed to heavy fractions, a relatively large amount of Z-A1AT distributed to heavy fractions, whereas smaller amounts of WT-A1AT were recruited to heavy fractions. Experiments were performed at least three times for all tested conditions.

(F) Co-immunoprecipitation of ERAD complexes from microsomes of polarized primary human nasal epithelial cells homozygous for Z mutation of A1AT. Derlin2 or K8 were immunoprecipitated with anti-Derlin2 or anti-K8 antibodies, respectively (see Methods section) and proteins of interest were detected using corresponding antibodies (Sel1, Hrd1, K8, Derlin2). Negative controls with unspecific mouse IgG (Ms IgG) and extracts, as well as with anti Derlin2 / K8 antibody and LMNG buffer were applied.

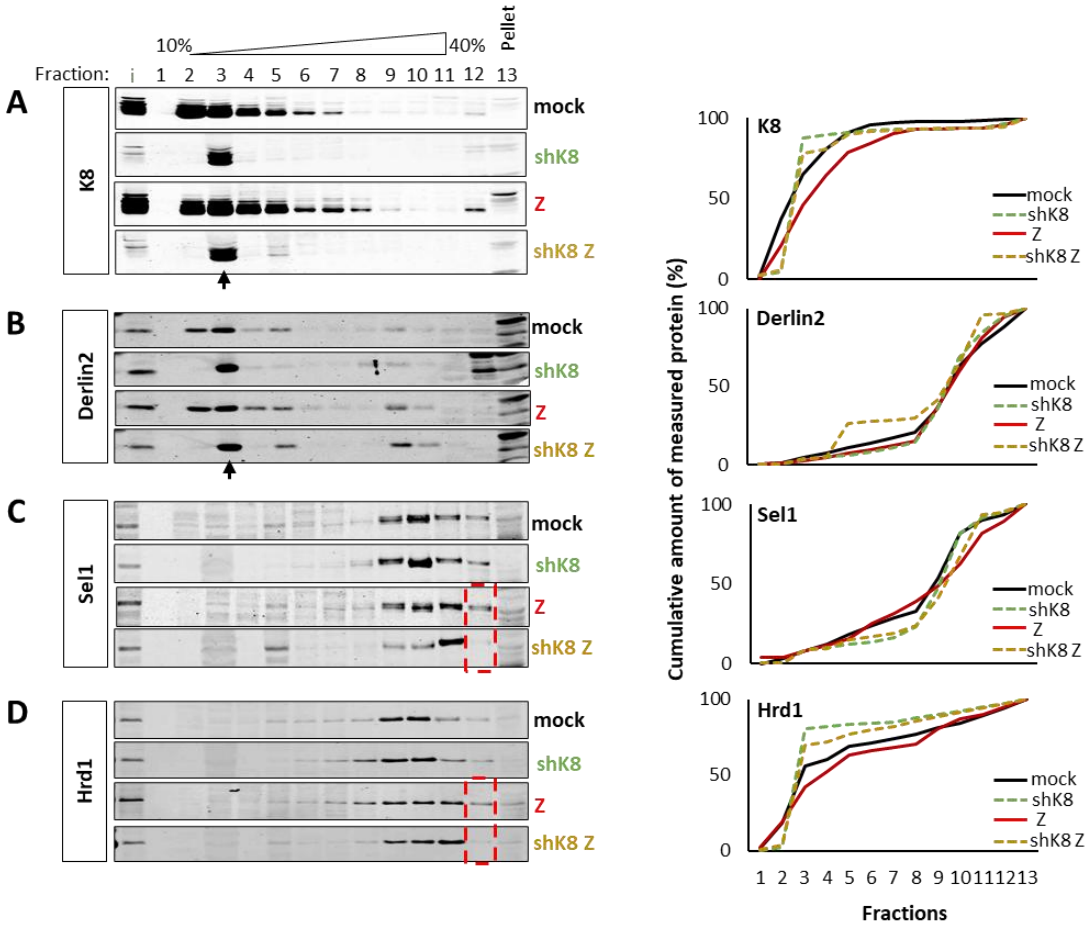

988

989 **Figure 4.** Silencing K8 affects ERAD complexes formation.

990 Sucrose gradient fractionation of the ERAD complexes. HeLa cells expressing normal
991 (mock and Z-A1AT) and decreased level of K8 (shK8 and shK8 Z-A1AT). Protein
992 samples from cells were sedimented over a 10 - 40% sucrose gradient. K8 (A), Sel1
993 (B), Hrd1 (C), Derlin-2 (D) were detected by immunoblotting with respective
994 antibodies. Black arrows correspond to ERAD complexes containing K8 and Derlin2
995 formed in shK8 cells, red dashed lined boxes correspond to high-density ERAD
996 complexes formed in presence of K8 and Z-A1AT (Z-A1AT cells) but missing in
997 shK8 Z-A1AT cells. Quantifications represent results shown in the corresponding
998 images on the left and are expressed as cumulative amount of measured protein (%) to
999 demonstrate the overall shift.

1000

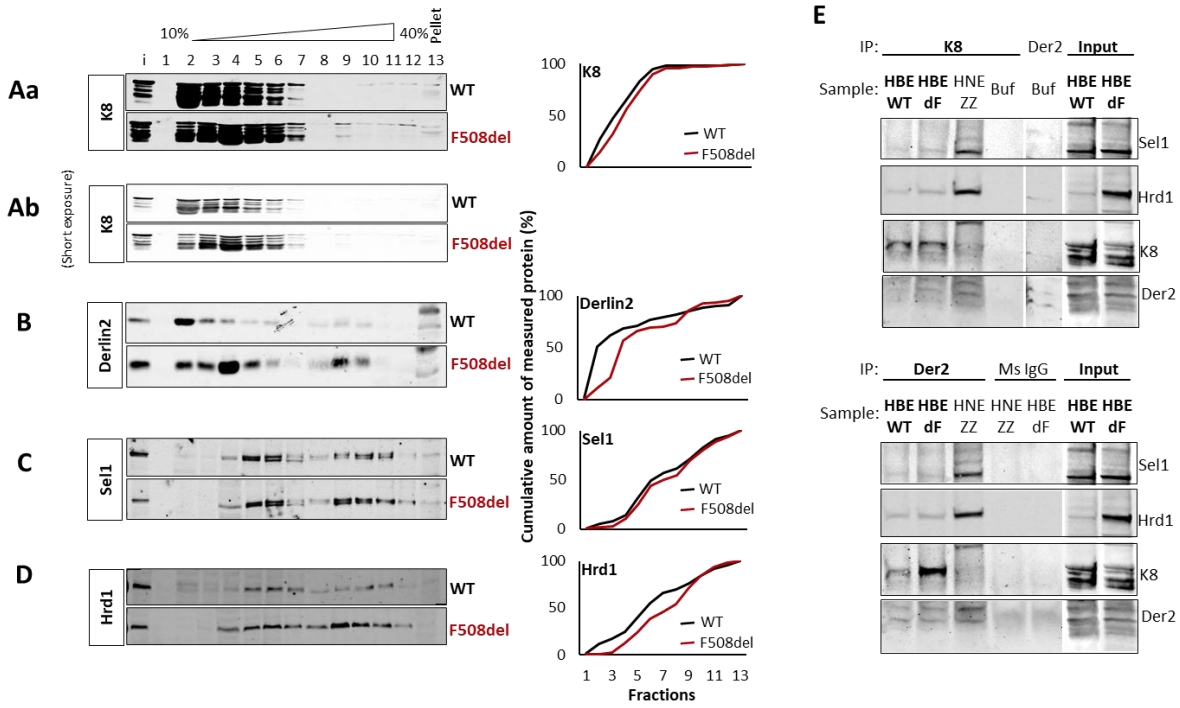

Figure 5. K8 is recruited to the ERAD complexes upon overexpression of misfolded F508del-CFTR.

16HBE cells expressing WT-CFTR and F508del-CFTR, as indicated, were lysed in 1% w/v LMNG and sedimented over a 10 - 40% w/v sucrose gradient. Levels of K8, Hrd1, Sel1, Derlin-2, were detected by immunoblotting. Representative images are shown. Quantifications represent results shown in the corresponding images on the left and are expressed as cumulative amount of measured protein (%) to demonstrate the overall shift. Experiment was performed three times.

(E) Co-immunoprecipitation of ERAD complexes from microsomes of 16HBE cells expressing WT- or F508del-CFTR. Derlin2 or K8 were immunoprecipitated with anti-Derlin2 (top panel) or anti-K8 antibodies (bottom panel), respectively (see Methods section) and proteins of interest were detected using corresponding antibodies (Sel1, Hrd1, K8, Derlin2). Negative controls with unspecific mouse IgG (Ms IgG) and extracts, as well as with anti Derlin2 / K8 antibody and LMNG buffer were applied.

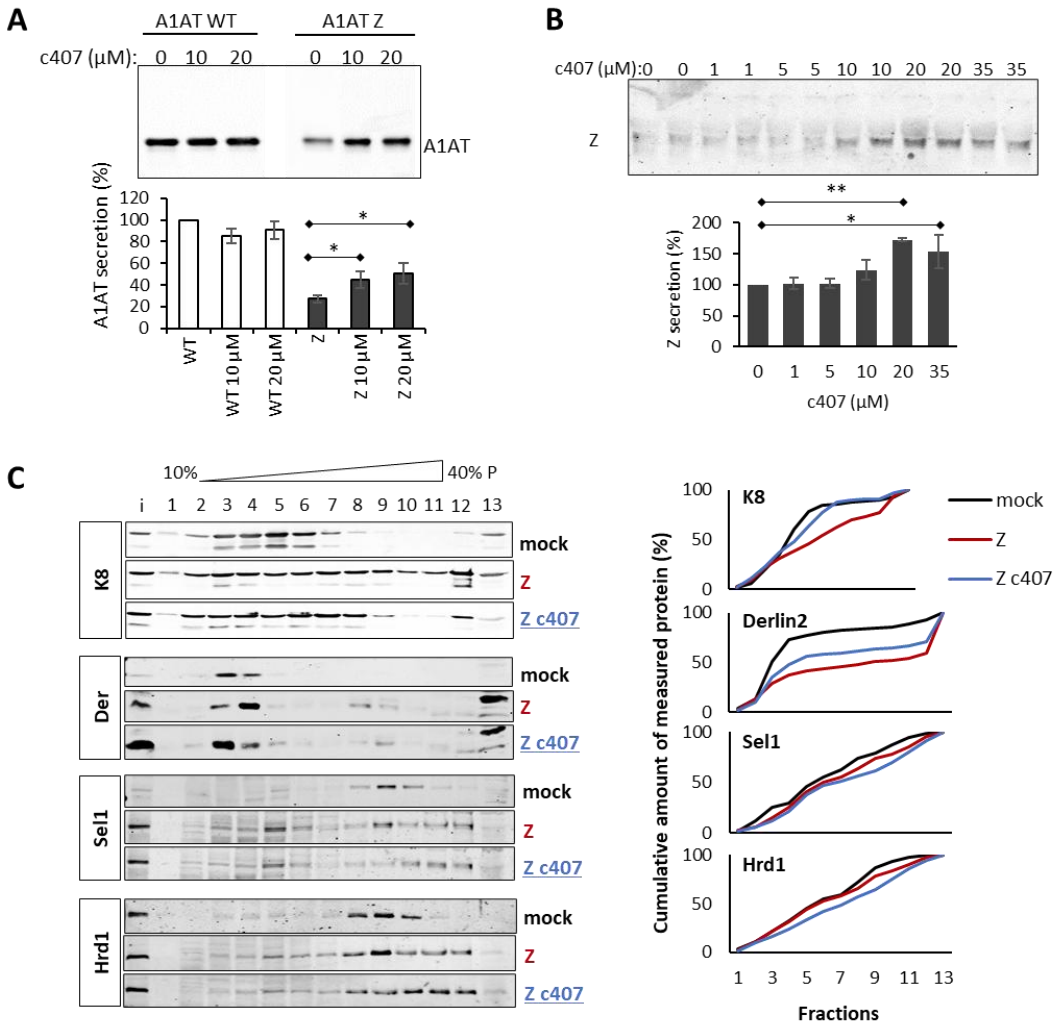

Figure 6. Compound c407 increases secretion of Z-A1AT from HeLa and primary HNE cells through modulating K8-contianing ERAD complexes.

(A) Quantification of WT-A1AT and Z-A1AT secretion level from HeLa cells upon treatment with c407 (10 and 20) and vehicle (0). Cells were treated with c407 at concentrations of 10 and 20 μM for 24 h. The representative WB analysis image shows A1AT secreted into the medium.

(B) Quantification of Z-A1AT secretion level from primary HNE cells upon treatment with c407 (1, 5, 10, 20 and 35) and vehicle (0). Cells were treated with c407 at concentrations of 1, 5, 10, 20 and 35 μM f or 14 days as pre-treatment and for 24 h for

test of secretion. The representative WB analysis image shows A1AT secreted into the medium.

(C) Sucrose gradient fractionation results upon c407 treatment. HeLa cells were transfected with Z-A1AT (Z) and treated with c407 at concentration of 20 μM or vehicle for 48 h, as indicated. Levels of K8, Hrd1, Sel1, and Derlin-2 were detected by immunoblotting in all fractions. Representative images are shown. Quantifications represent results shown in the corresponding images on the left and are expressed as cumulative amount of measured protein (%) to demonstrate the overall shift. Experiment was performed three times.

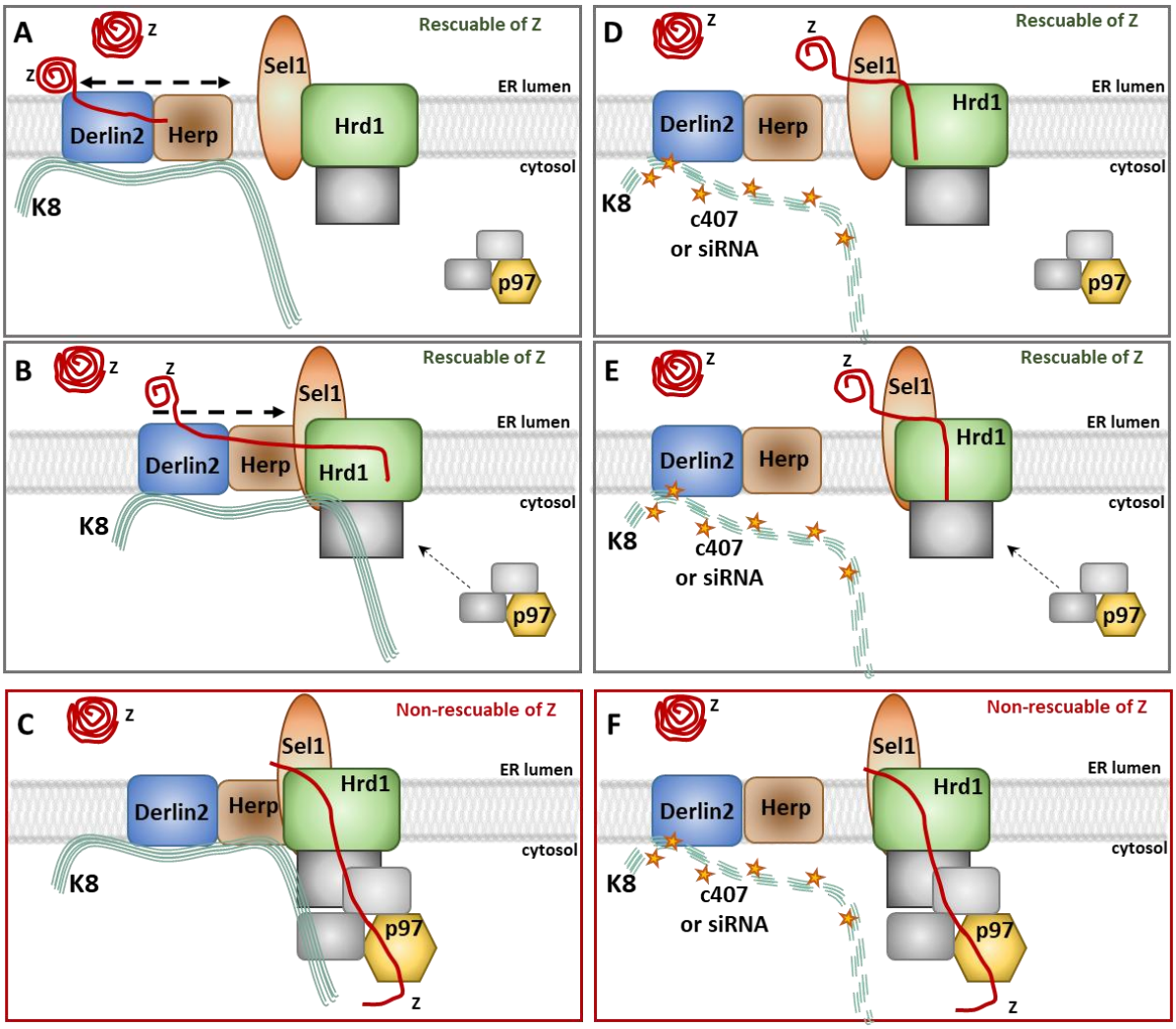

Figure 7. Model of K8 recruitment to the ERAD complexes at the ER membrane - hypothesis. (Adapted from Christianson and Ye).

Normal K8 recruitment to the ERAD complexes:

(A) K8 as a scaffolding platform in constant complex with Derlin2. Z-A1AT is recognised and recruited for retrotranslocation and ubiquitination. Stage rescuable for Z-A1AT secretion (upon Hrd1 or K8 down-regulation). Low density fractions complexes containing Derlin2 (module 2A in **Supp. Fig. 1**).

(B) K8 facilitates complexing with Hrd1/Sel1. Retrotranslocation of ubiquitinated Z-A1AT is initiated. Stage rescuable for Z-A1AT secretion (upon Hrd1 or K8 down-regulation). Medium

to high-density fractions complexes containing Derlin2, Sel1 and Hrd1 (modules 2A+2B in **Supp. Fig. 1**).

(C) Z-A1AT is being dislocated from the ER lumen to the cytosol. Dislocation stage no rescuable for Z-A1AT secretion (upon p97 inhibition). Hypothetic higher-order complexes containing Derlin2, Sel1, Hrd1 and p97.

Decreased or no recruitment of K8 to the ERAD complexes upon c407 molecule treatment or siRNA against K8:

(D) K8-Derlin2 complex maintained (low-density fractions) even with residual K8. However, K8-dependent scaffolding of higher-order complexes is affected. Recruitment of Z-A1AT for retrotranslocation and ubiquitination is reduced. ER-luminal Z-A1AT is secreted.

(E) K8-Derlin2 is not recruited to form complexes with Hrd1/Sel1. The shRNAK8 decreases Sel1 and Hrd1 recruitment to high-order complexes. By contrast, c407 treatment of cells do not change Hrd1 and Sel1 recruitment to higher-order complexes. Retrotranslocation initiation and ubiquitination of Z-A1AT is reduced. ER-luminal Z-A1AT is secreted.

(F) Z-A1AT dislocation to the cytosol is reduced. ER-luminal Z-A1AT is secreted.

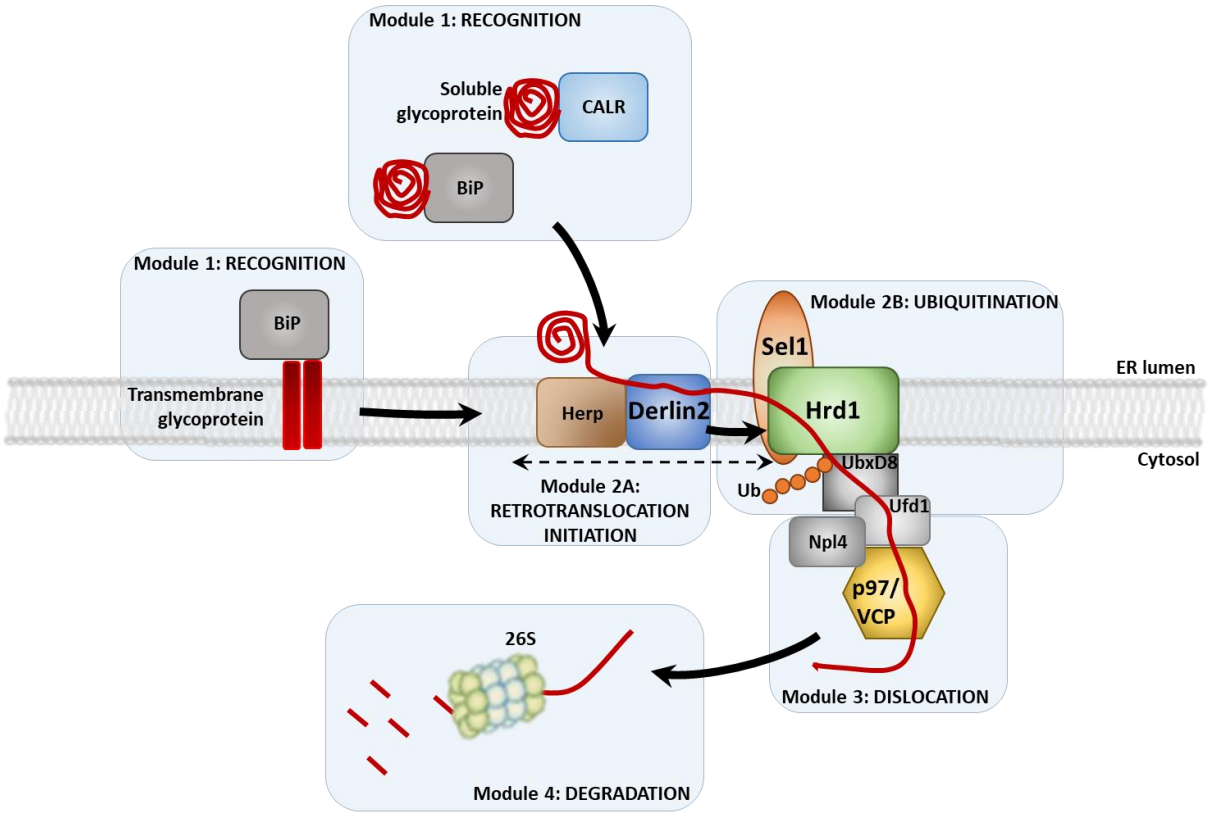

Supplementary Figure 1. Schematic representation of the mammalian ERAD pathway. **(Adapted from Christianson and Ye)**

Multiple ERAD proteins are organised into several modules. In general, proteins in the same module tend to form stable interactions, whereas proteins belonging to different modules dynamically bind with each other. Module 1 – Recognition: degradation substrates are bound to various chaperone proteins and glycosylation/deglycosylation factors, such as BiP and Calreticulin. Substrate recognition mechanisms vary depending on the type of substrate whether soluble or transmembrane and folded or misfolded. Module 2A – Retrotranslocation initiation: with substrate unfolding assured mainly by multifunctional Derlin proteins. Derlins participate in the transmembrane pore formation together with other proteins, i.e. Hrd1 E3 ubiquitin ligases. Module 2B – Ubiquitination: ubiquitin conjugation is mediated by E3 ubiquitin ligases including Hrd1 coupled to substrate recognition protein Sel1, and RNF185. Module 3 – Dislocation: extraction of the polypeptide from the ER membrane *via* the

p97/VCP ATPase complex providing a pulling force. Dislocated polypeptides are targeted to the 26S proteasome for degradation (Module 4 – Degradation). The arrows indicate the flow of the substrates. The dashed line-arrow indicates the recruitment or dissociation of Derlin2 from complexes of module 2B.

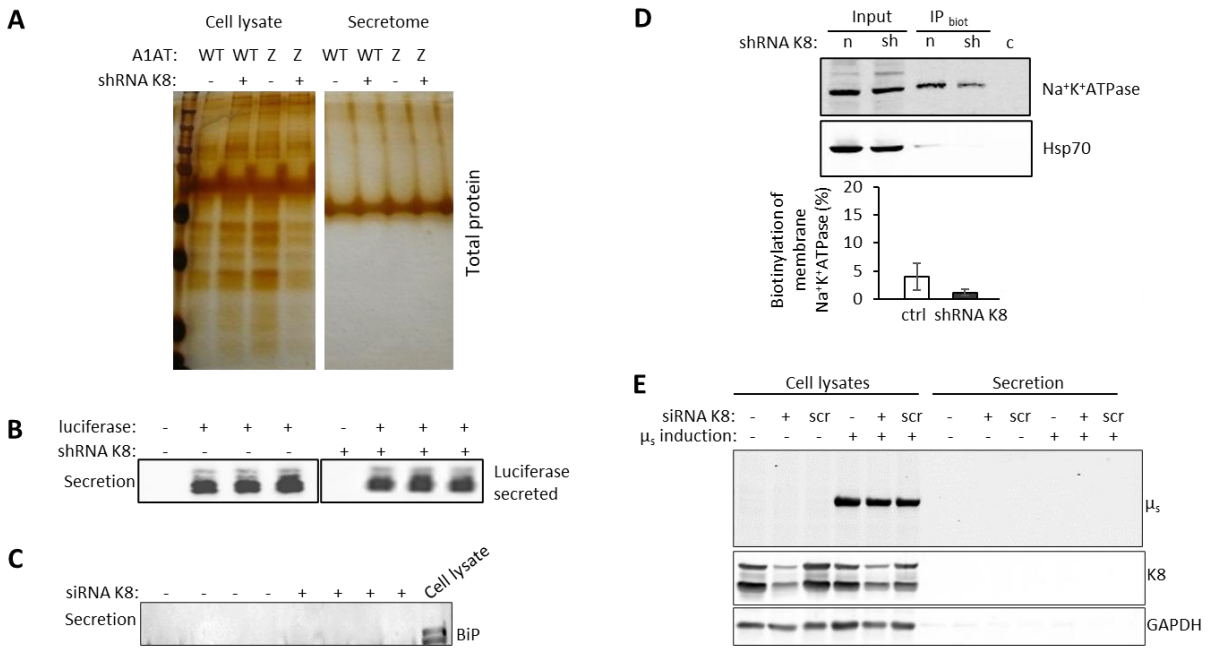

F

ER proteins	Secretory proteins
BiP	protein S100-A9, -A16, -A14
Calreticulin	Glypican-1, Glypican-5
Calumenin	multiple immunoglobulin superfamily members
	Alpha-fetoprotein
	Insulin-degrading enzyme

Supplementary Figure 2. K8 silencing does not influence global secretory trafficking.

(A) Silver-stained gel represents the cell lysates total protein content and the secretome protein content for shK8 and control HeLa cells.

(B) Transfected *Gaussia* luciferase secretion level from shK8 and control HeLa cells analysed using WB.

(C) Test of secretion of ER protein, BiP, from shRNA K8 and control HeLa cells.

(D) Surface biotynilation of Na^+K^+ATPase in shK8 and control HeLa cells.

(E) Test of secretion of μ_s (Mif 0.5 nM for 24 h) from shRNA K8 and control HeLa cells.

(F) ER and secretory proteins whose content in the secretome of HeLa cells upon K8 silencing did not change.

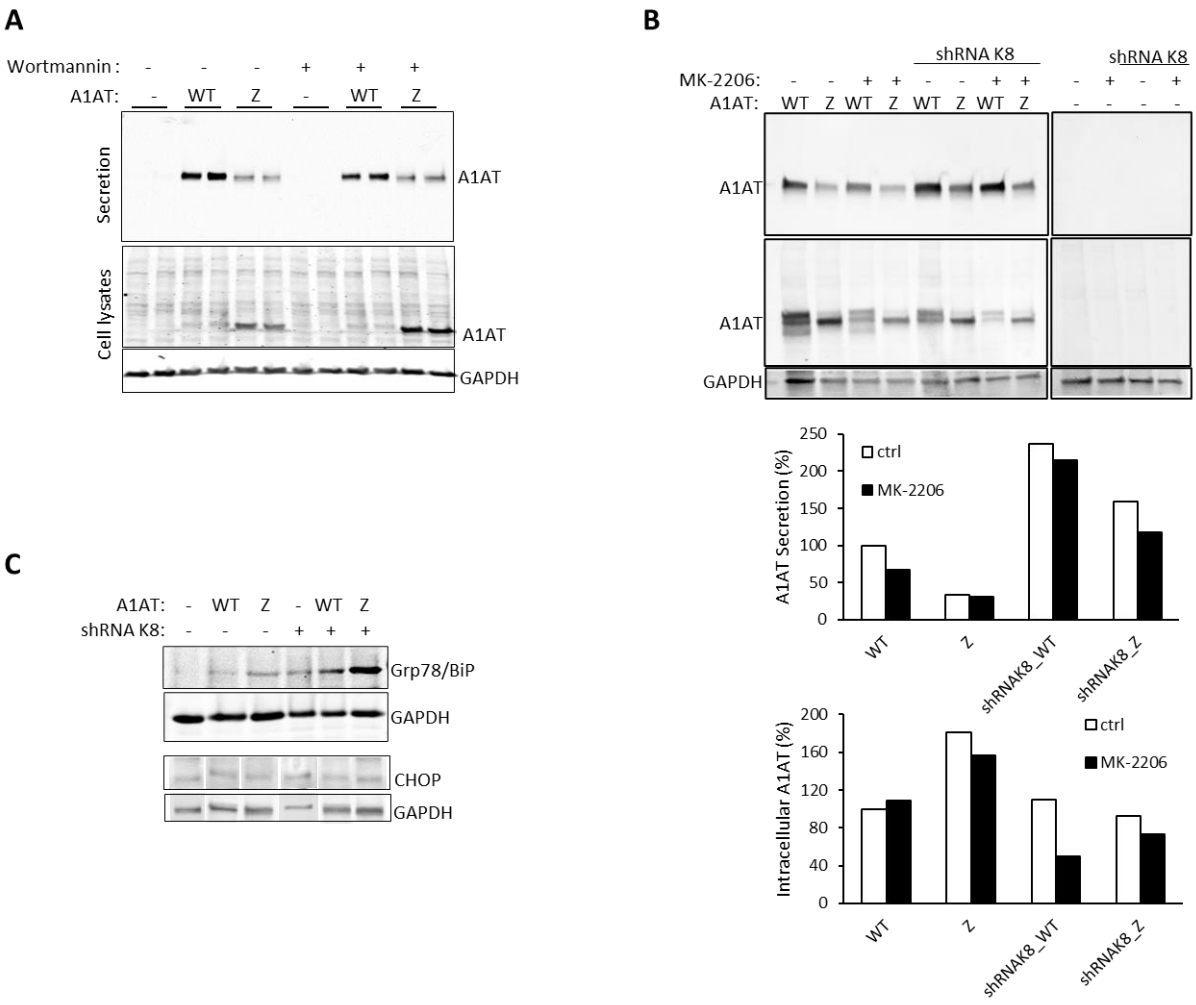

1120

1121 **Supplementary Figure 3.** K8 silencing increase ER stress in HeLa cells expressing Z-A1AT.

1122 Autophagy inhibition does not give the rescue of secretion.

1123 **(A)** Western blot analysis of secreted and intracellular WT- /Z-A1AT after HeLa cells

1124 treatment with Wortmannin (1 μM) for 20 h.

1125 **(B)** Effect of Akt inhibitor MK-2206 (5 μM for 20 h, autophagy inductor) on WT- / Z-A1AT

1126 secretion.

1127 **(C)** Western blot analysis of Grp78/BiP and CHOP expression levels in shK8 and control

1128 HeLa cells.

1129

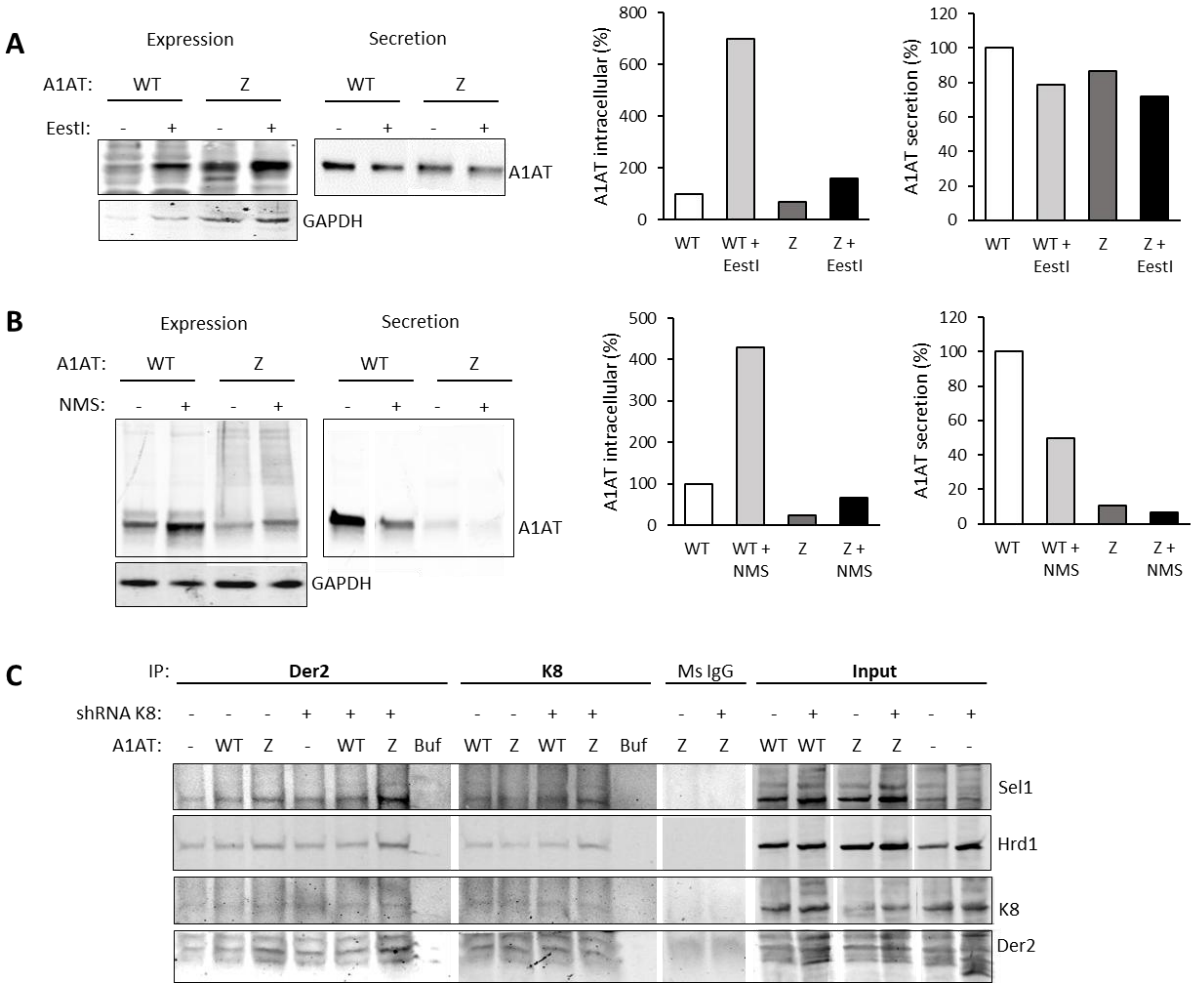

Supplementary Figure 4. (Related to Figure 2) Effect of p97 inhibition with EestI and NMS-873 inhibitors on A1AT secretion and accumulation in HeLa cells.

Representative WB immunodetection and quantification of WT- /Z-A1AT expression and secretion from HeLa cells in DMSO control conditions and upon treatment with EestI (10 μM) for 7 hours (A) and NMS-873 (1μM) for 20 hours (B).

Co-immunoprecipitation of ERAD complexes (**C)** from microsomes of HeLa cells transfected with WT or Z-A1AT. Derlin2 or K8 were immunoprecipitated with anti-Derlin2 or anti-K8 antibodies, respectively (see Methods section) and proteins of interest were detected using corresponding antibodies (Sel1, Hrd1, K8, Derlin2). Negative controls with unspecific mouse IgG (Ms IgG) and extracts, as well as with anti Derlin2 / K8 antibody and LMNG buffer were applied.

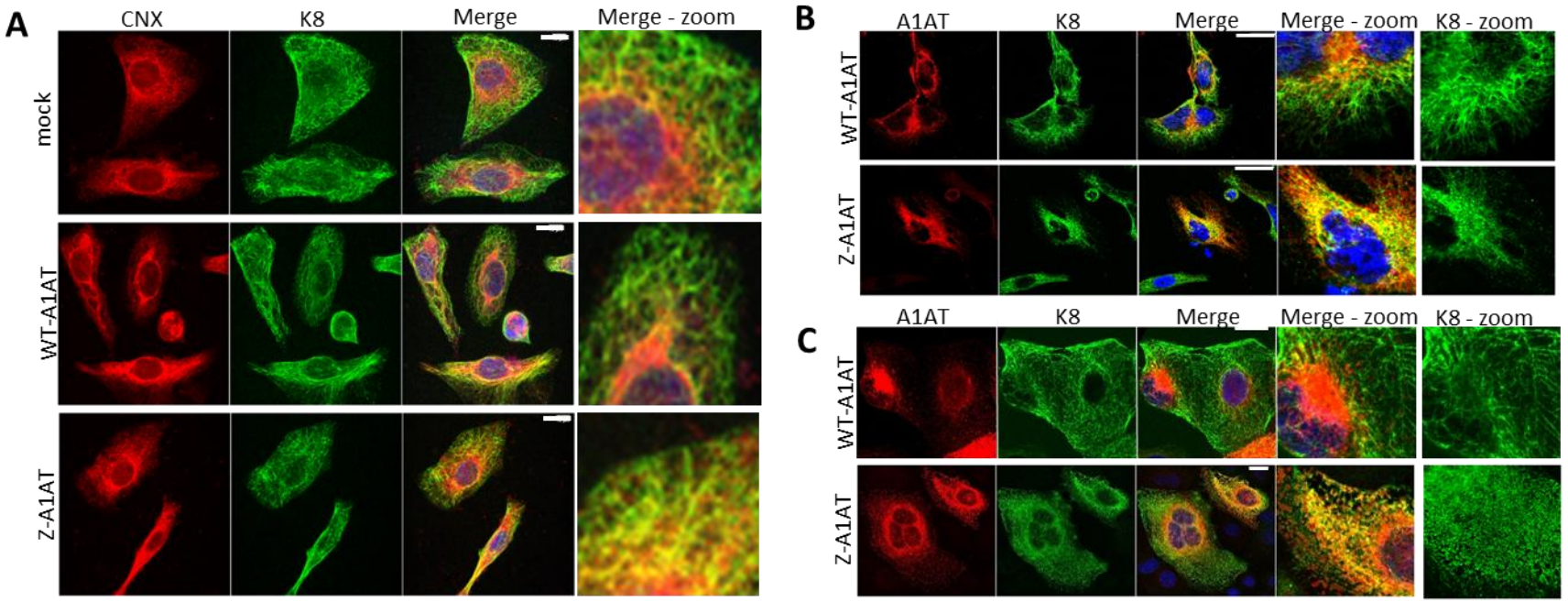
A
CNX
K8
Merge
Merge - zoom
mock
WT-A1AT
Z-A1AT
B
A1AT
K8
Merge
Merge - zoom
K8 - zoom
WT-A1AT
Z-A1AT
C
A1AT
K8
Merge
Merge - zoom
K8 - zoom
WT-A1AT
Z-A1AT

1142

Supplementary Figure 5. K8 redistributes to the ER upon expression of Z-A1AT in HeLa and primary HBE cells.

(A) Immunocytochemistry of A1AT and Calnexin (CNX), the ER marker, in mock-, WT-A1AT- or Z-A1AT-transfected HeLa cells. Representative images are shown. Scale bar = 20 μM.

(B) Immunocytochemistry of A1AT and K8 in HeLa cells transfected with WT-A1AT or Z-A1AT. Representative images are shown. Scale bar = 20 μM.

(C) Immunocytochemistry of A1AT and K8 in the primary HBE cells from the WT-homozygous donor and Z-homozygous patient, grown on microscopy slides. Representative images are provided. Scale bar = 20 μM.

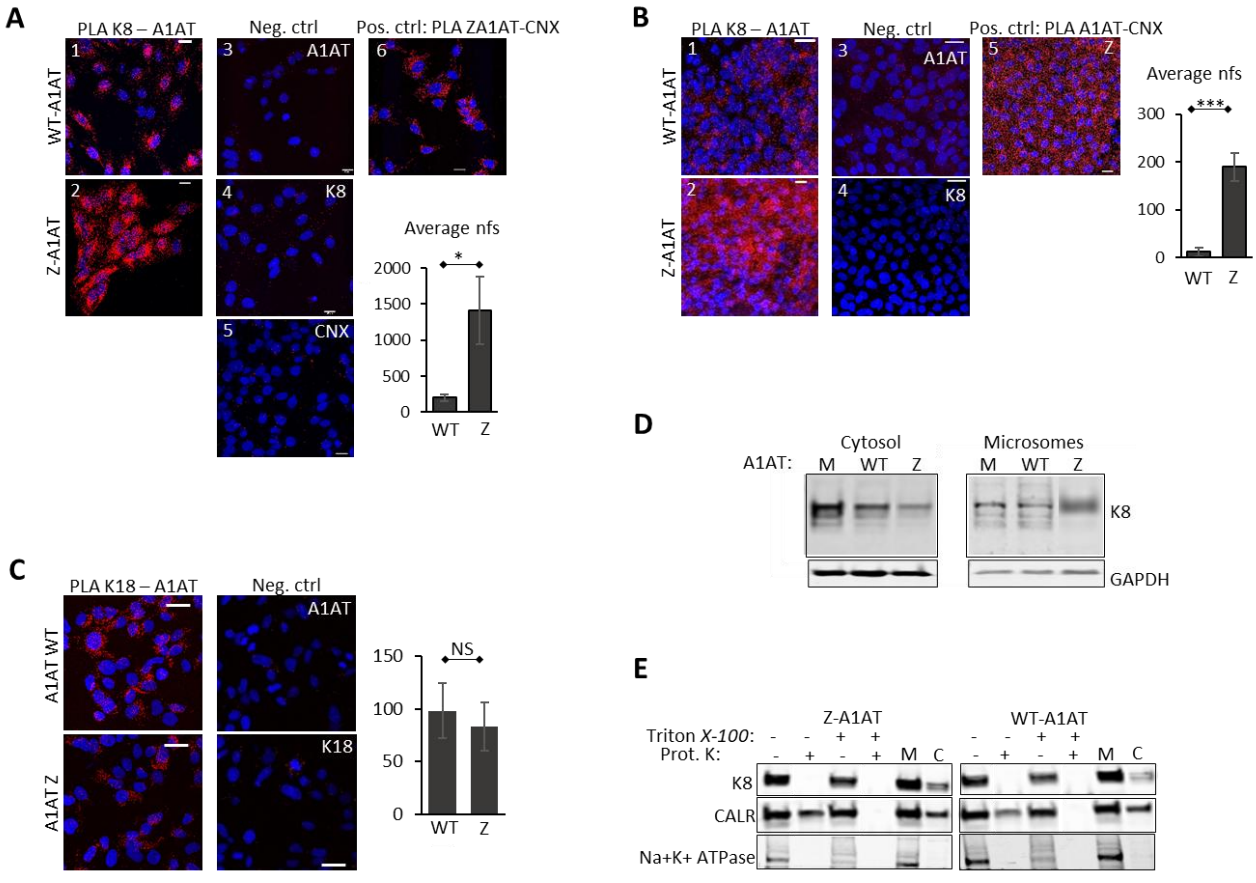

Supplementary Figure 6. K8 localizes in the close proximity to the ER membranes.

(A) Proximity ligation assay for K8 and A1AT in HeLa cells (images 1 and 2). Images on the right represent negative controls for single primary antibodies (images 3-A1AT, 4-K8 and 5-CNX) and positive control PLA for known interaction between Z-A1AT and Calnexin (image 6-Z-A1AT-CNX). Quantification represents an average number of fluorescent spots (nfs) / cell.

(B) Proximity ligation assay for K8 and A1AT in primary HBE cells (images 1 and 2). Images on the right represent negative controls for single primary antibodies (images 3-A1AT, 4-K8) and positive control PLA for known interaction between Z-A1AT and Calnexin (CNX) (image 5). Quantification represents an average number of fluorescent spots (nfs) / cell.

(**C**) Proximity ligation assay for K18 and A1AT in HeLa cells. Quantification represents an average number of fluorescent spots (nfs) / cell.

(D) Immunodetection of K8 and GAPDH in cytosolic and microsomal fractions of mock- (M), WT-A1AT- (WT), and Z-A1AT-transfected (Z) HeLa cells. Representative images of WB detection.

(E) HeLa cells derived microsomes were treated with Proteinase K (125 μg/ml) alone and Triton X-100 (0.5%) followed by Proteinase K. Microsomes were prepared using homogenisation of HeLa cells in an isotonic buffer and sequential centrifugations. Half of the volume was pre-treated with Triton X-100 (0.5%) and both types of samples were incubated with Proteinase K (125 μg/ml) at 37°C. The levels of degradation of K8, ER Calreticulin and transmembrane Na^+K^+ATPase were evaluated using WB and compared to untreated samples with Proteinase K. Samples M ctrl – microsomes (pellet of 100,000 g; C ctrl – cytosolic fraction (supernatant 100,000 g). Representative results are shown for cells expressing WT-A1AT or Z-A1AT.

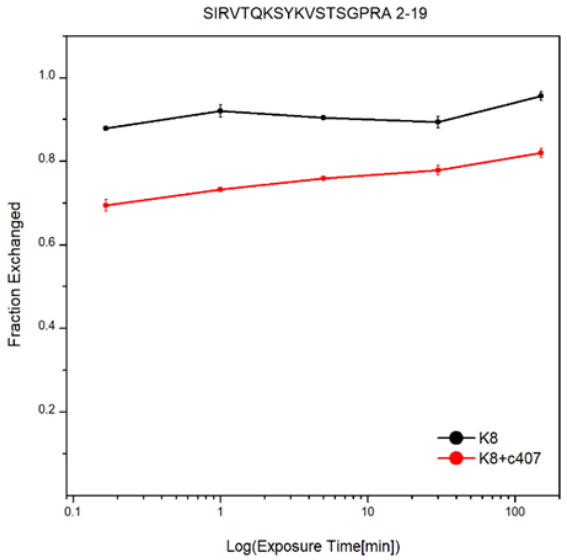
SIRVTQKSYKVSTSGPRA 2-19
Fraction Exchanged
Log(Exposure Time[min])
K8
K8+c407

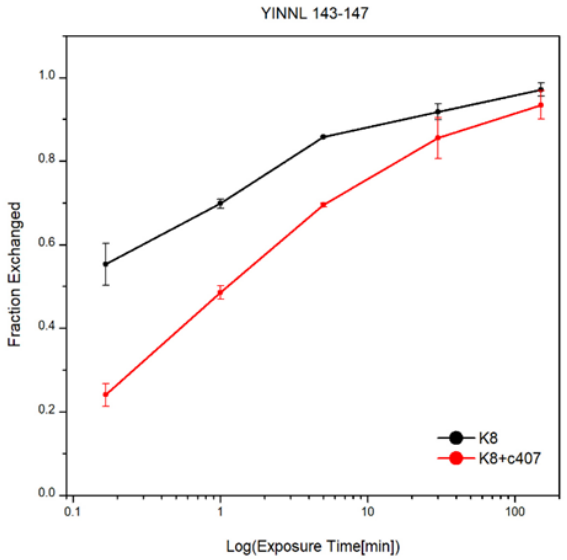
YINNL 143-147
Fraction Exchanged
Log(Exposure Time[min])
K8
K8+c407

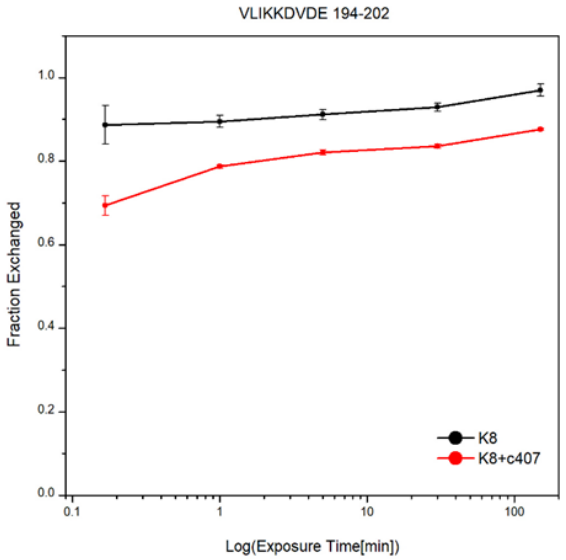
VLIKKDVDE 194-202
Fraction Exchanged
Log(Exposure Time[min])
K8
K8+c407

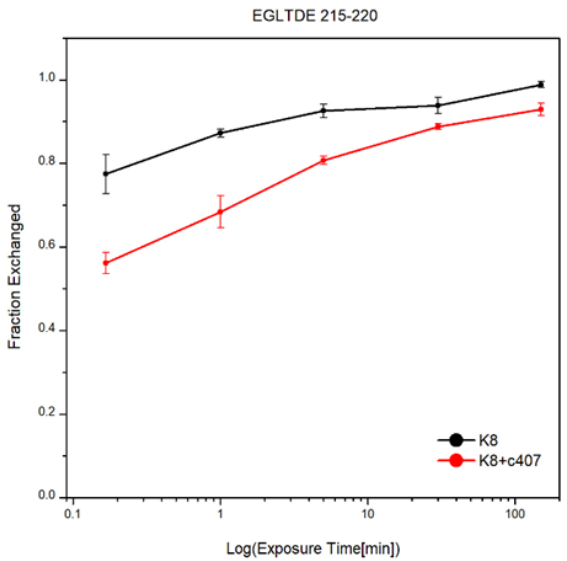
EGLTDE 215-220
Fraction Exchanged
Log(Exposure Time[min])
K8
K8+c407

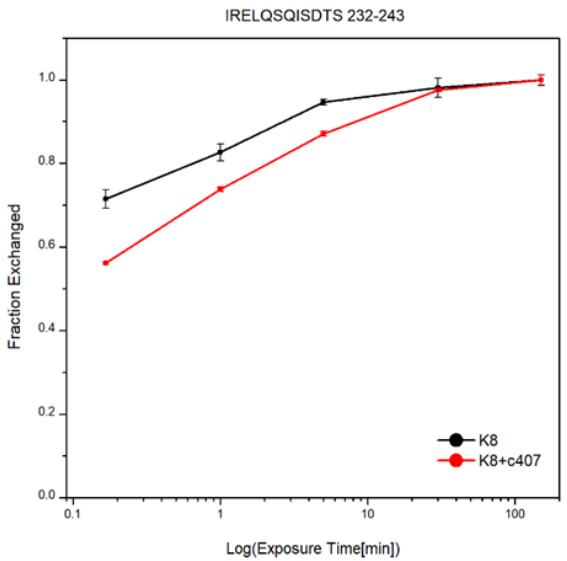
IRELQSQISDTS 232-243
Fraction Exchanged
Log(Exposure Time[min])
K8
K8+c407

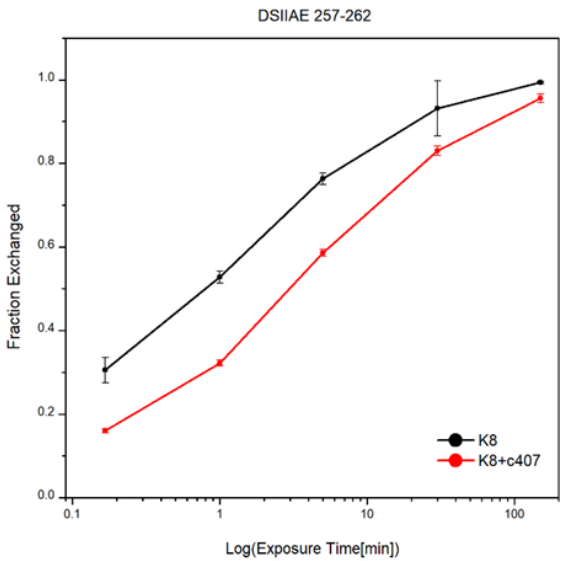
DSIIAE 257-262
Fraction Exchanged
Log(Exposure Time[min])
K8
K8+c407

1189

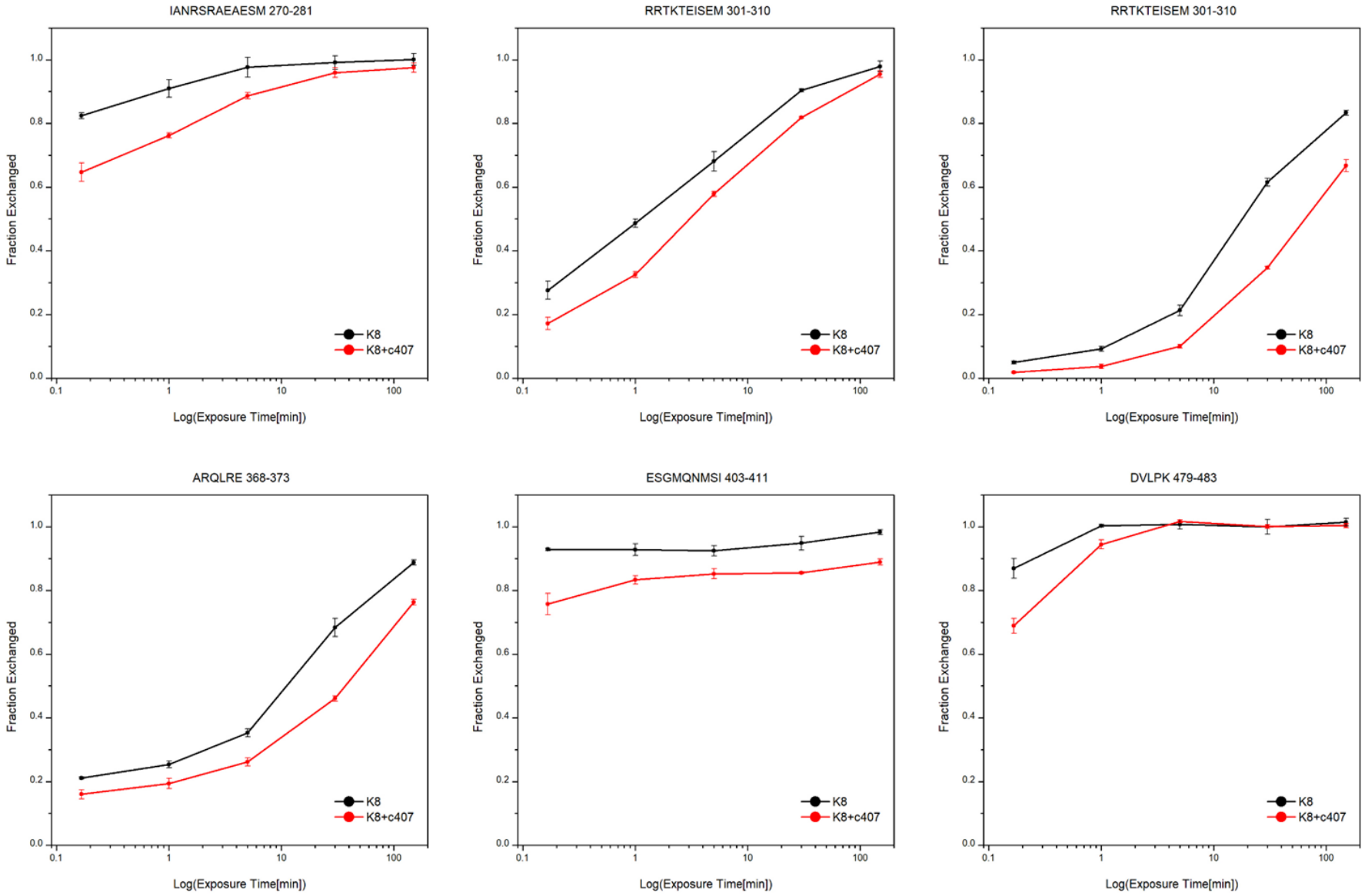
IANRSRAEAESM 270-281
RRTKTEISEM 301-310
RRTKTEISEM 301-310
ARQLRE 368-373
ESGMQNMSI 403-411
DVLPK 479-483
Fraction Exchanged
Log(Exposure Time[min])
K8
K8+c407

1190

Supplementary Figure 7 A and B. Kinetic plots of all the identified peptides from K8, depicting the fraction exchanged as a function of time.

The unbound, apo state is shown in black, while the bound, K8-c407 complex is shown in red. Error bars represent the standard deviation of three independent experiments.

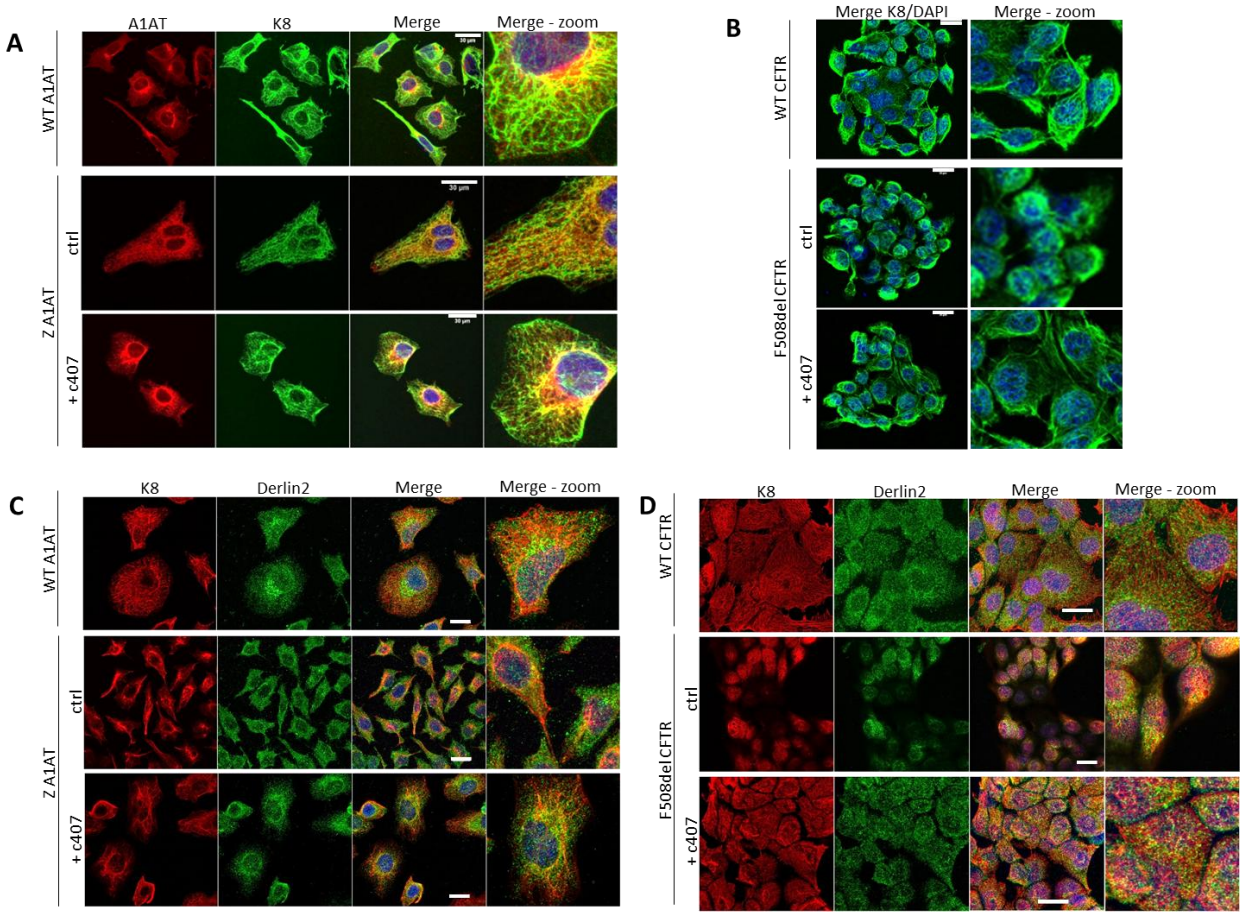

Supplementary Figure 8. Structure of K8 filament network in cells expressing misfolded protein after treatment with c407 molecule.

(A) Immunocytochemistry staining of A1AT (red) and K8 (green) in HeLa cells transfected with WT- or Z-A1AT treated or not with c407 (20 µM) for 24h. Representative images are shown. Scale bar = 30 µM.

(B) Immunocytochemistry staining of K8 (green) in 16HBE cells expressing WT- or F508del-CFTR treated or not with c407 (20 µM) for 24h. Representative images are shown. Scale bar = 20 µM.

(C) Immunocytochemistry staining of K8 (red) and Derlin2 (green) in HeLa cells transfected with WT- /Z-A1AT treated or not with c407 (20 µM) for 24h. Representative images are shown. Scale bar = 20 µM.

(D) Immunocytochemistry staining of K8 (red) and Derlin2 (green) in 16HBE cells expressing WT- or F508del-CFTR treated or not with c407 (20 μM) for 24h. Representative images are shown. Scale bar = 20 μM.

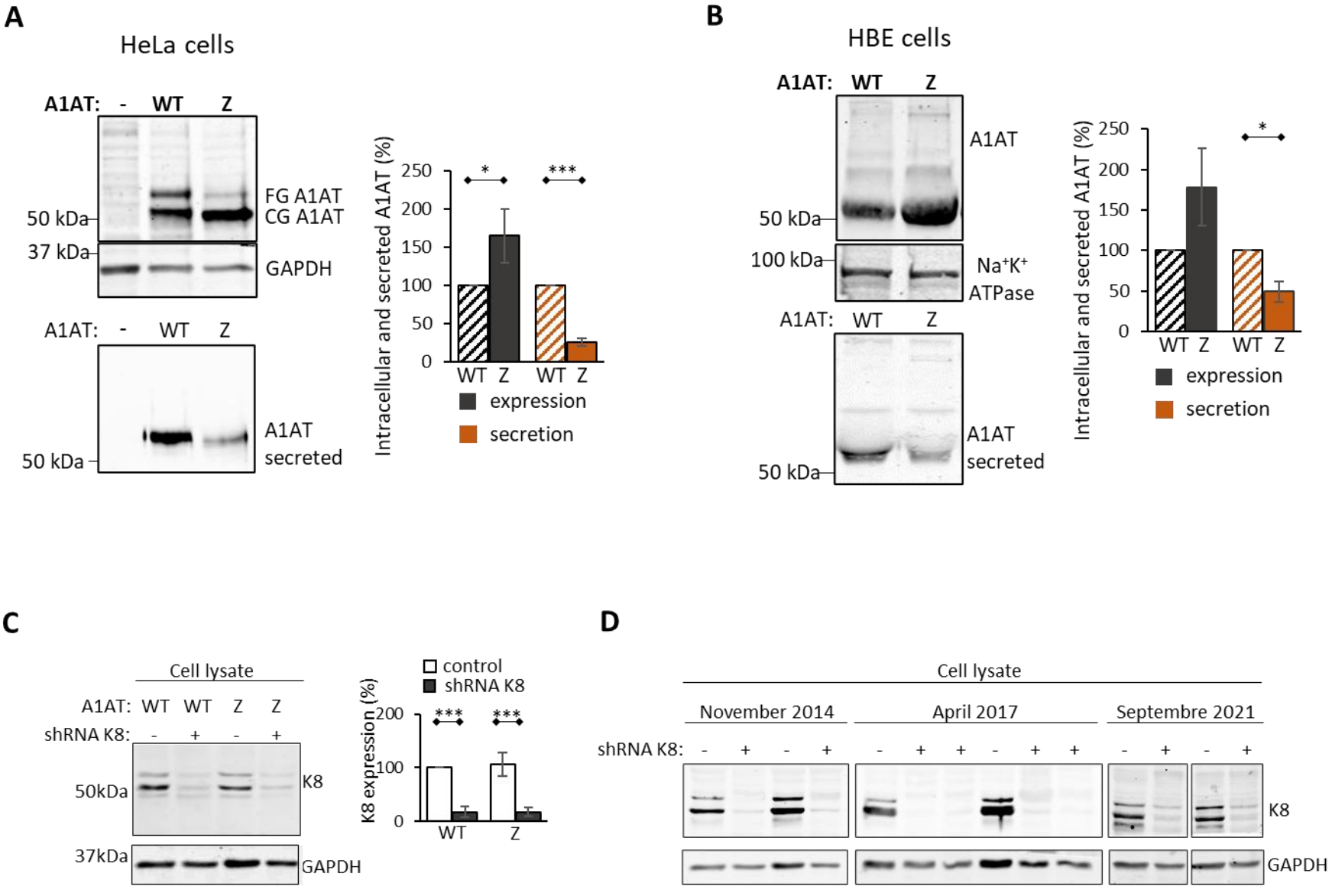
A
HeLa cells
A1AT: - WT Z
50 kDa
37 kDa
FG A1AT
CG A1AT
GAPDH
A1AT: - WT Z
50 kDa
A1AT
secreted
Intracellular and secreted A1AT (%)
250
200
150
100
50
0
*
***
WT Z WT Z
expression
secretion
B
HBE cells
A1AT: WT Z
A1AT
50 kDa
100 kDa
Na+K+
ATPase
A1AT: WT Z
A1AT
secreted
50 kDa
Intracellular and secreted A1AT (%)
250
200
150
100
50
0
*
WT Z WT Z
expression
secretion
C
Cell lysate
A1AT: WT WT Z Z
shRNA K8: - + - +
50kDa
K8
37kDa
GAPDH
control
shRNA K8
K8 expression (%)
200
100
0
***
***
WT
Z
D
Cell lysate
November 2014
April 2017
Septembre 2021
shRNA K8: - + - + - + + - + + - + - +
K8
GAPDH

1226

Supplementary Figure 9. (Related to Material and methods) Expression of WT-A1AT and Z-A1AT in HeLa and primary HBE cells – characterisation of cells

(A) Expression and secretion of WT-A1AT and Z-A1AT in HeLa cell cultures after transfection with pcDNA3 plasmids coding for WT-A1AT or Z-A1AT. Top membranes - cell extracts probed for A1AT expression and GAPDH as a loading control. Bottom membrane – culture media without FCS after 24 h incubation with transfected HeLa cells were probed for the presence of A1AT. FG – fully-glycosylated, CG – core-glycosylated. Representative images are included. Quantification of nine independent experiments (* $p \leq 0.05$, *** $p \leq 0.0001$).

(B) Expression and secretion levels of WT-A1AT and Z-A1AT in primary HBE cell cultures isolated from two healthy controls (wt/wt A1AT) and two homozygous Z-A1AT individuals. Top membranes - cell extracts probed for expression of A1AT and Na^+K^+ATPase as the loading control. Bottom membrane - culture media without FCS after 24 h incubation with HBE cells were analysed for the presence of A1AT. Representative images are demonstrated. Quantification of four experiments for each subject (* $p \leq 0.05$).

(C) Western blot detection and quantification for intracellular K8 and GAPDH in cells with normal (shRNAK8-) and decreased (shRNAK8+) levels of K8 expression.

(D) Validation of the HeLa shRNA K8 cell line by verifying K8 protein level of expression at three different time points (as indicated). Western blot detection or intracellular K8 and GAPDH in cells with normal (shRNAK8-) and decreased (shRNAK8+) levels of K8 expression.